# Emergent Non-Reciprocal Circularly Polarized Emission from an Organic Thin Film

*Francesco Zinna, Gianluigi Albano,[‡] Andrea Taddeucci, Tony Colli, Laura Antonella Aronica, Gennaro Pescitelli, Lorenzo Di Bari**

Dr. F. Zinna, Dr. G. Albano, A. Taddeucci, T. Colli, Dr. L. A. Aronica, Prof. G. Pescitelli, Prof. L. Di Bari
Dipartimento di Chimica e Chimica Indistriale, Università Di Pisa, via Moruzzi 13, 56124, Pisa, Italy

Dr. F. Zinna, Dr. L. A. Aronica, Prof. G. Pescitelli, Prof. L. Di Bari
CISUP, Centro per l'Integrazione della Strumentazione dell'Università di Pisa, Lungarno Pacinotti 43, 56126, Pisa, Italy

‡ Current address: Dipartimento di Chimica, Università degli Studi di Bari "Aldo Moro", Via Edoardo Orabona 4, 70126 Bari, Italy

**Email:** lorenzo.dibari@unipi.it

**Keywords:** CPL, chirality, chiral optoelectronics, CP-OLED, π-conjugated compounds

## Abstract

Controlling circularly polarized (CP) emission is key for both fundamental understanding and applications in the field of chiral photonics and electronics. Here, a completely new way to achieve this goal is presented. A luminescent thin film, made from a chiral conjugated phenylene bis-thiophenylpropynone able to self-assemble into ordered structures, emits highly circularly polarized light with opposite handedness from its two opposite faces. Such emergent non-reciprocal behaviour in CP emission, so far unprecedented, represents a fundamental advance, opening new opportunities in design, preparation and applications of CP emitting materials.

**Main text**

Harnessing circularly polarized (CP) emission from molecular systems opens the way to new opportunities in chirality sensing,[1] chiral templating,[2] CP-electrochemiluminescence[3] and CP-OLEDs.[4] In the flourishing field of chiral photonics and electronics, new ways for more thorough control of CP light generation are desirable.[5] To widen the scope of applications of CP emitting systems, a material capable of CP emission with opposite handedness depending of the direction of the emitted light would have major implications. This would require an apparent breaking of CP emission reciprocity, that is inverting the handedness of CP light upon reversal of the emitted light wavevector.[6] So far, organic materials featuring non-reciprocal CP emission have never been explored. Here we show that upon thin film deposition, a designed chiral molecule self-assembles in aggregates displaying a very high degree of emergent non-reciprocal CP absorption and emission, making it possible to achieve a new type of CP emitting functional material.

Recently thin films prepared with selected chiral π-conjugated systems have proven an effective scaffold for non-reciprocal CP absorption,[7] that is an almost complete inversion of the handedness of the CP component preferentially transmitted by the two opposite faces of the sample. This is practically observed by flipping the film sample by 180° with respect to light propagation axis, while showing negligible *emergent* linear dichroism (*LD*) or linear birefringence (*LB*). Such phenomenon is made possible by the peculiar aggregates formed by the molecules upon film deposition and annealing, whereby their linear anisotropies average to zero on the large (from 1 mm on) scale, while their combination does not.[6, 8]

On the other hand, non-reciprocal CP emission, although theoretically expected, was never observed, probably due to the lack of compounds able to self-assemble in suitably ordered structures and to display significant emission in aggregate form.[9] Despite this lack of experimental evidence so far, such properties would be extremely useful in terms of

dissymmetry factor enhancement thanks to its underlying mechanism, tunability and spatial and directional control of CP emission. This would provide a functional material capable of opposite handedness CP emission from the two opposite faces, without resorting to stacking different layers such as additional chiral coatings,[10] acting as opposite CP-sensitive band rejection filter. Indeed, CP generation and control is key to achieve the forecasted applications such as optical data storage,[11] CP-laser[12] and better performing CP-OLEDs[13] furthering the emergent field of chiral electronics and photonics.

Given the context, in order to experimentally demonstrate emergent non-reciprocal CP emission, we synthesised a π-conjugated molecule, PTPO (phenylene bis-thiophenylpropynone, Scheme 1), decorated with chiral aliphatic side-chains deriving from naturally occurring β-citronellol[14] (see supplementary information for synthetic details). Such compound displays an extended electronic conjugation together with a relatively rigid structure of the conjugated core. The intrinsic chirality of the compound alone is not sufficient to give rise to any significant chiroptical property of the isolated (solvated) molecules, in absorption (electronic circular dichroism, ECD) or in emission (CP emission), but it is necessary to lead the aggregation into ordered dissymmetric structures upon thin film deposition, where ECD and possibly CP emission may become relevant.[15]

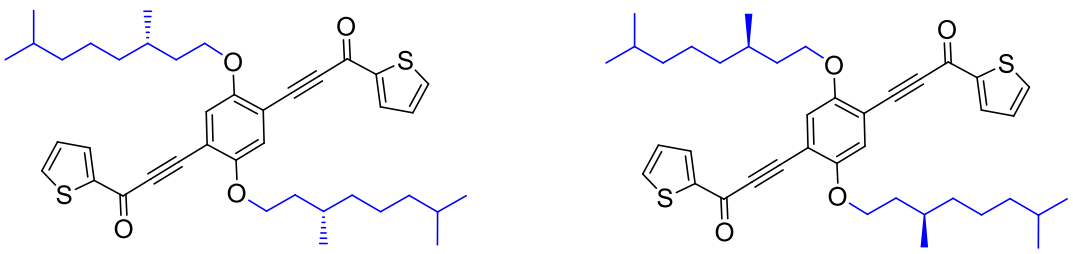


**Scheme 1.** Structures of (*S*,*S*)-PTPO (left) and (*R*,*R*)-PTPO (right).

With such compound in hand, we prepared spin-coated films of PTPO, deposited onto a transparent glass substrate, under optimized conditions (Figure S1). Then, the films underwent thermal annealing at 80 °C (compound melting point 95-97 °C), to allow for the necessary molecular mobility. This treatment spontaneously leads to a thermodynamically favourable arrangement of the molecules in the thin film,[5b, 16] which is responsible for all the chiroptical properties herein described. The films appeared homogeneous and semi-transparent (OD around 0.4 at 465 nm, thickness 300 nm).

Firstly, we noticed that PTPO thin films displayed a bright emission in the green region ($\lambda_{max}$ 512 nm, Figure S2), making them good candidates for CP emission measurements. Then, in order to prove non-reciprocal CP emission, the following experiment was designed: the film was excited using a non-polarized 0° illumination between excitation and emission and the luminescence was collected from the same face of the film (Figure S3). In this way, it is possible to reliably measure independently the luminescence circular polarization stemming from the two faces of the film: with the coated side facing the excitation source/detector (*forward* configuration) or, oppositely, with the uncoated face oriented towards the excitation source/detector (*backward* configuration). Therefore, in these two configurations, the wavevector of the emitted light propagates in opposite directions with respect to the film surface (Figure 1d). Indeed, when (*S*,*S*)-PTPO films were placed facing the detector (forward), an intense negative CP emission signal ($\lambda_{max}$ 505 nm) was detected throughout the emission spectrum.

Interestingly, when the circular polarization of the emission was measured in the backward configuration (with the uncoated side of the film facing the detector), an opposite (positive), signal was obtained. The signal was mirror-like with respect to the forward CP emission, that is it displayed the same shape and the same maximum wavelength (Figure 1b).

The degree of CP emission was quantified using the dissymmetry factor $g_{lum} = 2(I_L-I_R)/(I_L+I_R)$, where $I_L$ and $I_R$ are the left and right CP component of the emission respectively. Importantly, forward CP and backward CP emission displayed opposite but same order of magnitude $g_{lum}$ factors: -0.15 ± 0.01 for forward configuration and +0.09 ± 0.02 for backward one, calculated on the CPL maximum (505 nm, Figure 1b)). Such figures, on the upper range for aggregated (non-cholesteric) films prepared from organic materials,[9b][17] are due to the peculiar mechanism generating the CP emission (see below). The $g_{lum}$ factor is fairly constant throughout the emission region, but it shows a maximum around 475 nm (forward $g_{lum}$ = -0.23 ± 0.03, backward $g_{lum}$ = +0.12 ± 0.03) suggesting the presence of more than one contribution under the relatively simple emission spectrum (Figure 1b). Such properties were measured on several samples from independent preparations to check for consistency and reproducibility (see error bars in Figure 1b). This confirmed the robustness of both film preparation and measurement techniques employed.

At this point, care was taken to demonstrate that such non-reciprocal CP effect in emission, was free from instrumental artefacts or spurious effects. Fluorescence linear anisotropy was measured and determined to be negligible with respect to the total measured signal (below 3%, see Figure S4). Such contribution would be reciprocal (i.e. invariant in forward and backward configuration) but sign-changing upon sample rotation around the optical axis. As a further confirmation, CP emission spectra were recorded at different film rotations to ensure that no significant variations were present (Figure S5).

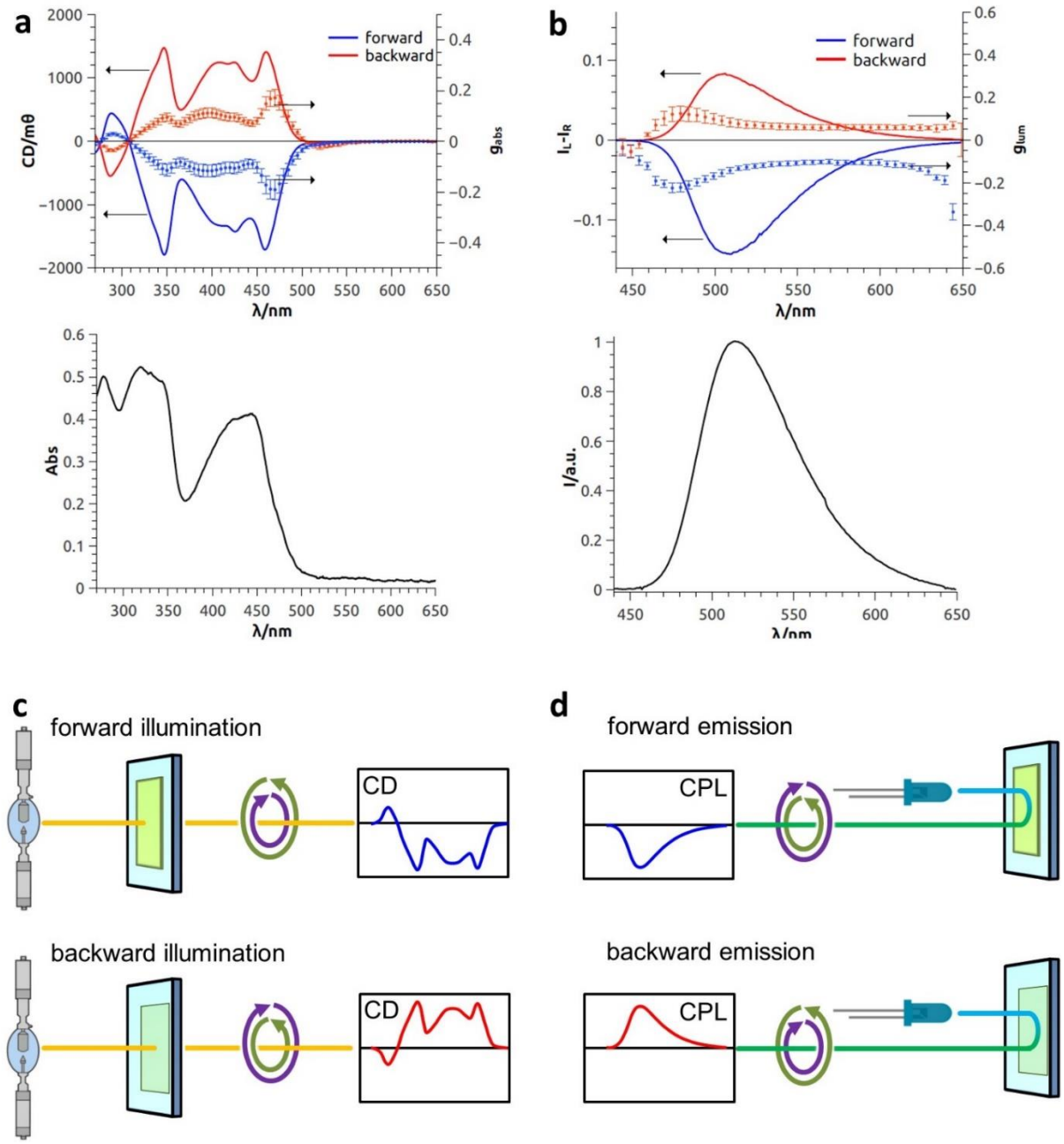


**Figure 1. a:** ECD, $g_{abs}$ values and absorption spectrum of thermally annealed (*S*,*S*)-PTPO films in forward and backward configuration. **b:** CP emission, $g_{lum}$ values and emission spectrum of the film in forward and backward configuration (excitation 365 nm). The error bars on $g_{abs}$ and $g_{lum}$ values represent one standard deviation calculated over 5 replicates). Bottom: cartoon illustrating forward/backward measuring conditions for ECD (**c**) and CP emission (**d**).

The chiroptical analysis was then carried out in absorption. ECD spectra were recorded on the same films in forward (coated side facing the illumination) and backward (coated side facing the detector) configuration (see Figure 1c). Again, the direction of the irradiating wavevector is opposite in the two configurations. As expected, (*S*,*S*)-PTPO, showed predominantly negative

bands in the forward configuration, while it was completely inverted (mainly positive bands) in backward configurations. In both configurations the ECD signals recorded were particularly intense. In fact, the absorption dissymmetry factor $g_{abs}$: $2(A_L-A_R)/(A_L+A_R)$ ($A_L$ and $A_R$ being the left and right CP component of the absorption) was -0.19 ± 0.03 and +0.17 ± 0.03 at 465 nm for forward and backward configuration respectively (Figure 1c). Again, a rotation of the sample around its optical axis did not show any significant variation in the ECD spectrum indicating no significant net contribution from linear components (Figure S6). Moreover, no significant trace of scattering is visible in the ECD or in the absorption spectra.

To further confirm the phenomenon, the enantiomer compound (*R*,*R*)-PTPO was synthesized (Scheme 1) and its films investigated in the same manner. As expected, ECD and CP emission measured in forward configuration were positive, that is opposite with respect to (S,S)-PTPO, while they were negative in backward configuration. On the other hand, no significant change in the spectral shape of ECD and CP emission was observed (Figure S7). Small differences in the magnitude of $g_{abs}$ and $g_{lum}$ obtained with the two enantiomers are due to a lower optical purity of the starting (*R*)-β-citronellol with respect to the (*S*) enantiomer.

For completeness, the chiroptical behaviour and morphological characteristics of the non-annealed films were studied as well. ECD spectra show almost identical shape and sign in forward and backward configurations. On the other hand, CP emission spectra show already some hint of non-reciprocal emission: forward CP emission spectrum displays a negative band (for (*S*,*S*)-PTPO) with a $g_{lum}$ around $-9\cdot10^{-2}$ at 503 nm, while in backward configuration no significant signal is recorded at 503 nm, but a small opposite band is visible at 470 nm ($+1\cdot10^{-2}$, see Figure S8 and S9).

The morphological characterisation confirms the effect of the thermal annealing. Non-annealed films display a surface entirely formed by needle-like crystals (100x500 nm), as visible in atomic force microscopy (AFM) and field emission scanning electron microscopy (FE-SEM) images (Figure S11). Upon thermal annealing, such features completely disappear, giving rise to step-terrace structures at (sub-)μm scale (see FE-SEM and AFM images, Figure 2b and S10).

At this point an explanation for the observed non-reciprocal behaviour was looked for. Analogously to non-reciprocal CP transmission,[6, 18] emergent non-reciprocal CP emission in the present sample may be rationalized taking into account the presence of a significant coupling between fluorescence linear anisotropy (*f*) and linear birefringence (*LB*) giving rise to an emergent circularly polarized emission.[5b] Such contribution is odd by wavevector inversion and therefore the film displays CP emission with opposite polarization from its two faces. This is not in contrast with the absence of a net fluorescence linear anisotropy from the sample, as the film may consist of several domains, each of them with a random orientation, effectively averaging out to zero the overall linear contribution. On the other hand, coupling between *f* and *LB* does not vanish out as it depends only on the reciprocal position of *f* and *LB* vectors and not by their orientation on the film surface.

Such view is strongly corroborated by optical and electron microscopy images of the films. FE-SEM images show that the film bulk is made of distinct grain-like domains (50-100 μm size), clearly separated by boundaries (Figure 2a). Each domain displays a clear orientation on the film surface, as indicated by the regular and persistent parallel striping pattern within each grain (Figure 2a and S10), compatible with locally non-vanishing *f* and *LB* (Figure 2c). On the other hand, each grain is randomly oriented with respect to the other ones, ensuring no net linear contribution in the emission. A clear birefringence pattern compatible with the size of the grains is observed as well in cross polarized optical microscopy (Figure 2e).

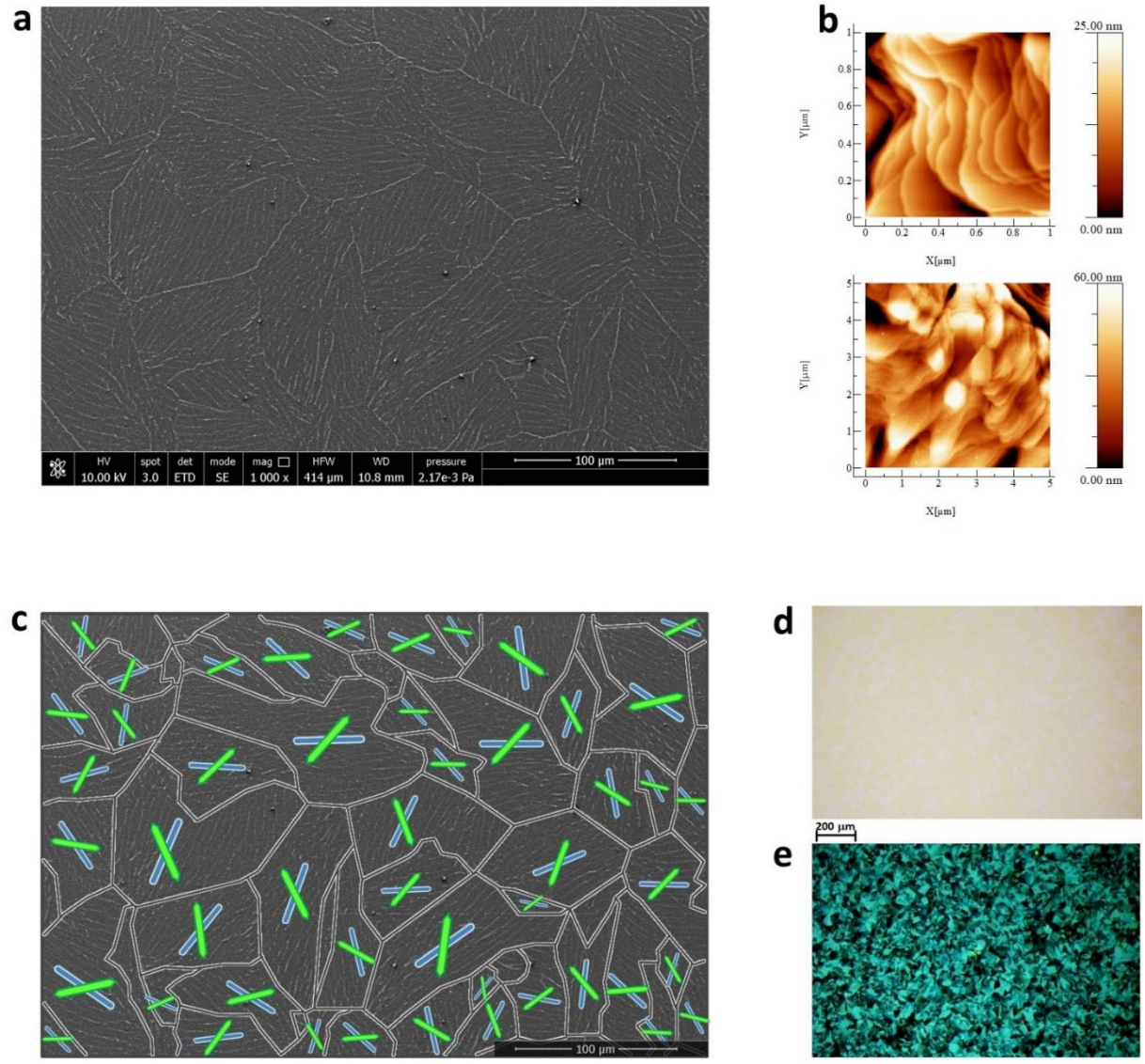


**Figure 2. a:** FE-SEM image of a thermally annealed film of (*S*,*S*)-PTPO. **b:** AFM images of portions of the film. **c:** cartoon showing an elaboration of the FE-SEM image, with grain boundaries highlighted and a pictorial representation of oriented *f* (green sticks) and *LB* (blue rods) within each grain; blue rods are oriented along the striping pattern. Bottom right: bright field (**d**) and crossed polarized (**e**) optical microscopy images of the film.

We are not unaware that a straightforward application of such type of materials may be in CP-OLEDs, where opposite forward and backward polarization may be beneficial in avoiding depolarization upon reflection on the device electrode (see discussion in supplementary information).[13, 19]

In conclusion, we have presented an unprecedented example of emergent non-reciprocal CP emission thanks to a molecule able to self-aggregates in thin film forming peculiar structures.

In the present example, front and back film surfaces display almost enantiomer-like behaviour in terms of circular polarization of emitted and absorbed light. This phenomenon is not related to commonly reported CP luminescence, but if carefully engineered and measured, it allows for control of optical activity in emission within the same thin film and we believe that materials displaying such properties will benefit the promising field of chiral electronics and photonics.

**Acknowledgments**

Financial support from Italian University and Research ministry (PRIN Project 20172M3K5N) is gratefully acknowledged. We thank CISUP - Centre for Instrumentation Sharing - University of Pisa, for FE-SEM (Dr Randa Anis Ishak) and AFM (Dr Massimiliano Labardi) analysis.

**Supporting Information**

Supporting Information is available from the Wiley Online Library or from the author.

**References**

[1] J. R. Brandt, F. Salerno, M. J. Fuchter, *Nat. Rev. Chem.* **2017**, *1*, 0045.

[2] J. Yeom, B. Yeom, H. Chan, K. W. Smith, S. Dominguez-Medina, J. H. Bahng, G. Zhao, W.-S. Chang, S.-J. Chang, A. Chuvilin, *Nat. Mater.* **2015**, *14*, 66.

[3] F. Zinna, S. Voci, L. Arrico, E. Brun, A. Homberg, L. Bouffier, T. Funaioli, J. Lacour, N. Sojic, L. Di Bari, *Angew. Chem. Int. Ed.* **2019**, *58*, 6952.

[4] D.-W. Zhang, M. Li, C.-F. Chen, *Chem. Soc. Rev.* **2020**, in press, doi: 10.1039/c9cs00680j

[5] a) Y. Yang, R. C. da Costa, D. M. Smilgies, A. J. Campbell, M. J. Fuchter, *Adv. Mater.* **2013**, *25*, 2624; b) D. Di Nuzzo, C. Kulkarni, B. Zhao, E. Smolinsky, F. Tassinari, S. C. Meskers, R. Naaman, E. Meijer, R. H. Friend, *ACS nano* **2017**, *11*, 12713; c) M. Schulz, J. Zablocki, O. S. Abdullaeva, S. Brück, F. Balzer, A. Lützen, O. Arteaga, M. Schiek, *Nat. Commun.* **2018**, *9*, 1; d) K. Baek, D.-M. Lee, Y.-J. Lee, H. Choi, J. Seo, I. Kang, C.-J. Yu, J.-H. Kim, *Light Sci. Appl.* **2019**, *8*, 1; e) Y. Yang, R. C. Da Costa, M. J. Fuchter, A. J. Campbell, *Nat. Photonics* **2013**, *7*, 634; f) G. Long,

R. Sabatini, M. I. Saidaminov, G. Lakhwani, A. Rasmita, X. Liu, E. H. Sargent, W. Gao, *Nat. Rev. Mater.* **2020**, in press, doi: 10.1038/s41578-020-0181-5.

[6] O. Arteaga, B. M. Maoz, S. Nichols, G. Markovich, B. Kahr, *Optics express* **2014**, *22*, 13719.

[7] a) G. Albano, M. Lissia, G. Pescitelli, L. A. Aronica, L. Di Bari, *Mater. Chem. Front.* **2017**, *1*, 2047; b) A. von Weber, D. C. Hooper, M. Jakob, V. K. Valev, A. Kartouzian, U. Heiz, *ChemPhysChem* **2019**, *20*, 62; c) G. Albano, F. Salerno, L. Portus, W. Porzio, L. A. Aronica, L. Di Bari, *ChemNanoMat* **2018**, *4*, 1059; d) G. Albano, M. Górecki, G. Pescitelli, L. Di Bari, T. Jávorfi, R. Hussain, G. Siligardi, *New J. Chem.* **2019**, *43*, 14584.

[8] Y. Shindo, Y. Ohmi, *J. Am. Chem. Soc.* **1985**, *107*, 91.

[9] a) Y. Sang, J. Han, T. Zhao, P. Duan, M. Liu, *Adv. Mater.* **2020**, *1900110*, in Pres, doi: 10.1002/adma.201900110; b) J. Kumar, T. Nakashima, T. Kawai, *J. Phys. Chem. Lett.* **2015**, *6*, 3445.

[10] B. Zhao, K. Pan, J. Deng, *Macromolecules* **2018**, *52*, 376.

[11] C. Wang, H. Fei, Y. Qiu, Y. Yang, Z. Wei, Y. Tian, Y. Chen, Y. Zhao, *Appl. Phys. Lett.* **1999**, *74*, 19.

[12] J. Jiménez, L. Cerdán, F. Moreno, B. L. Maroto, I. García-Moreno, J. L. Lunkley, G. Muller, S. de la Moya, *J. Phys. Chem. C* **2017**, *121*, 5287.

[13] F. Zinna, G. Pescitelli, L. D. Bari, *Chirality* **2020**, in press, doi:10.1002/chir.23217.

[14] J. H. K. K. Hirschberg, L. Brunsveld, A. Ramzi, J. A. J. M. Vekemans, R. P. Sijbesma, E. W. Meijer, *Nature* **2000**, *407*, 167.

[15] a) M. Liu, L. Zhang, T. Wang, *Chem. Rev.* **2015**, *115*, 7304; b) Y. Yang, Y. Zhang, Z. Wei, *Adv. Mater.* **2013**, *25*, 6039.

[16] L. Wan, J. Wade, F. Salerno, O. Arteaga, B. Laidlaw, X. Wang, T. Penfold, M. J. Fuchter, A. J. Campbell, *ACS Nano* **2019**, *13*, 8099.

[17] aK. Watanabe, Z. Sun, K. Akagi, *Chem. Mater.* **2015**, *27*, 2895; bB. Zhao, K. Pan, J. Deng, *Macromolecules* **2019**, *52*, 376.

[18] B. Kahr, J. Freudenthal, E. Gunn, *Acc. Chem. Res.* **2010**, *43*, 684.

[19] a) F. Zinna, U. Giovanella, L. Di Bari, *Adv. Mater.* **2015**, *27*, 1791; b) F. Zinna, M. Pasini, F. Galeotti, C. Botta, L. Di Bari, U. Giovanella, *Adv. Funct. Mater.* **2017**, *27*, 1603719.

Received: ((will be filled in by the editorial staff))
Revised: ((will be filled in by the editorial staff))
Published online: ((will be filled in by the editorial staff))

**Keywords:** CPL, chirality, chiral optoelectronics, CP-OLED, π-conjugated compounds

F. Zinna, G. Albano, A. Taddeucci, T. Colli, L. A. Aronica, G. Pescitelli, L. Di Bari*

**Emergent Non-Reciprocal Circularly Polarized Emission from an Organic Thin Film**

The thin film of a chiral π-conjugated phenylene derivative emits circularly polarized (CP) light with high degree of dissymmetry and opposite handedness from the two opposite faces of the film. Non-reciprocal CP emission is unreported so far, and it offers unprecedented opportunities in the design of CP emitting materials.

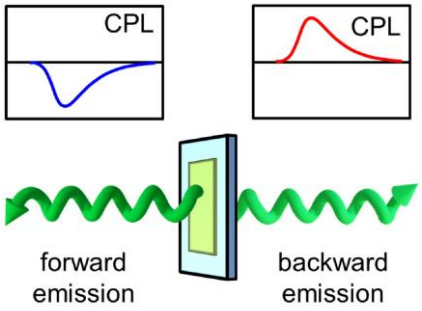

# Supporting Information

## Emergent Non-Reciprocal Circularly Polarized Emission from an Organic Thin Film

*Francesco Zinna, Gianluigi Albano,[‡] Andrea Taddeucci, Tony Colli, Laura Antonella Aronica, Gennaro Pescitelli, Lorenzo Di Bari**

# Synthetic procedures

## General information

Solvents were purified by conventional methods, distilled and stored under argon. (*S*)-(−)-β-citronellol and (*R*)-(+)-β-citronellol were purchased from Sigma Aldrich (for (*S*)-citronellol: 99.1 % purity (GC) and optical rotation (neat) -4.9; for *(R)*-citronellol: 97% purity (GC) and optical rotation (neat) +4.3*)*. All other chemicals were purchased from Sigma Aldrich or Alfa Aesar and used as received without further purification. Commercial grade solvents were purified by conventional methods, distilled and stored over activated molecular sieves under nitrogen atmosphere. All the operations under inert atmosphere were carried out using standard Schlenk techniques and employing dried nitrogen. Reactions conversion was monitored by thin-layer chromatography (TLC) analysis on pre-coated silica gel plates ALUGRAM® Xtra SIL G/UV254 (0.2 mm) purchased from VWR Macherey-Nagel. Column chromatography was performed with Fluka silica gel, pore size 60 Å, 70-230 mesh, 63-200 μm.

$^{1}$H-NMR and $^{13}$C-NMR spectra were recorded at room temperature in $CDCl_3$ or DMSO-$d_6$ solution with a Bruker Avance DRX 400 spectrometer, operating at a frequency of 400 MHz for $^{1}$H and 100 MHz for $^{13}$C, using the residual solvent peak as internal reference; chemical shifts (δ) values are given in parts per million (ppm) and coupling constants (J) in Hertz. Mass spectra were obtained with an Applied Biosystems-MDS Sciex API 4000 triple quadrupole mass spectrometer (Concord, Ont., Canada), equipped with a Turbo-V ion-spray (TIS) source. Elemental analyses were performed on a Elementar Vario Micro Cube CHN-analyzer.

## Procedures

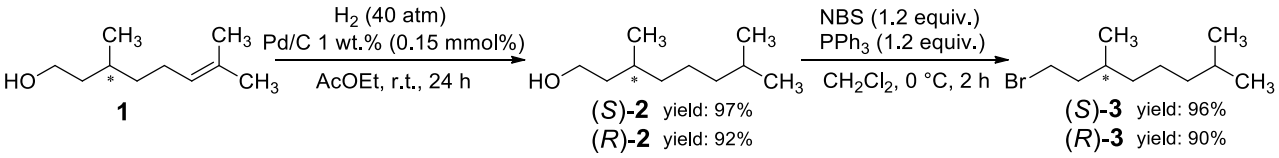


**Scheme S1**

### Synthesis of (*S*)-3,7-dimethyloctan-1-ol ((*S*)-2)[S1]

In a 95 mL stainless steel autoclave fitted with a Teflon inner crucible and a stirring bar, (*S*)-(−)-β-citronellol (*S*)-**1** (10.00 g, 64.0 mmol), AcOEt (30 mL) and Pd/C 1 wt.% (1.00 g, 0.15 mol%) were mixed together. The reactor was pressurized with $H_2$ (40 atm) and the mixture was stirred for 24 h at room temperature. After removal of excess $H_2$ (fume hood), the reaction

mixture was diluted with hexane, filtered through Celite and the solvent was removed under vacuum to give (*S*)-3,7-dimethyloctan-1-ol (*S*)-**2** (9.82 g, 97% yield) as a colourless oil which was used without further purification.

$^{1}$H-NMR (400 MHz, $CDCl_3$), δ (ppm): 0.83-0.87 (9H, m), 1.06-1.16 (3H, m), 1.18-1.30 (3H, m), 1.32-1.39 (1H, m), 1.43-1.62 (4H, m), 3.59-3.70 (2H, m). $^{13}$C-NMR (100 MHz, $CDCl_3$), δ (ppm): 19.60, 22.55, 22.66, 24.65, 27.93, 29.49, 37.35, 39.23, 39.96, 61.19.

**Synthesis of (*R*)-3,7-dimethyloctan-1-ol ((*R*)-2)**

According to the previous procedure, (*R*)-3,7-dimethyloctan-1-ol (*R*)-**2** (92% yield) was obtained starting from (*R*)-(+)-β-citronellol (*R*)-**1**.

**Synthesis of (*S*)-1-bromo-3,7-dimethyloctane ((*S*)-3)[S1]**

(*S*)-3,7-Dimethyloctan-1-ol (*S*)-**2** (8.69 g, 54.9 mmol) and triphenylphosphine (17.00 g, 64.8 mmol) were dissolved in $CH_2Cl_2$ (180 mL), then *N*-bromosuccinimide (10.96 g, 61.6 mmol) was added portion-wise to the solution at 0 °C. After stirring of the mixture for 2 h at 0 °C, the solvent was removed under vacuum and the solid residue was suspended in *n*-hexane. The mixture was stirred for 10 min at room temperature, then it was filtered through Celite and the solvent was removed under vacuum. The crude product was purified through column chromatography ($SiO_2$, *n*-hexane) yielding (*S*)-1-bromo-3,7-dimethyloctane (*S*)-**3** (11.66 g, yield 96%) as a colourless liquid.

$^{1}$H-NMR (400 MHz, $CDCl_3$), δ (ppm): 0.84-0.88 (9H, m), 1.05-1.17 (3H, m), 1.19-1.34 (3H, m), 1.44-1.56 (1H, m), 1.57-1.69 (2H, m), 1.81-1.90 (1H, m), 3.35-3.47 (2H, m). $^{13}$C-NMR (100 MHz, $CDCl_3$), δ (ppm): 18.94, 22.56, 22.66, 24.53, 27.93, 31.66, 32.09, 36.71, 39.16, 40.08.

**Synthesis of (*R*)-1-bromo-3,7-dimethyloctane ((*R*)-3)**

According to the previous procedure, (*R*)-1-bromo-3,7-dimethyloctane (*R*)-**3** (90% yield) was obtained starting from (*R*)-3,7-dimethyloctan-1-ol (**R**)-**2**.

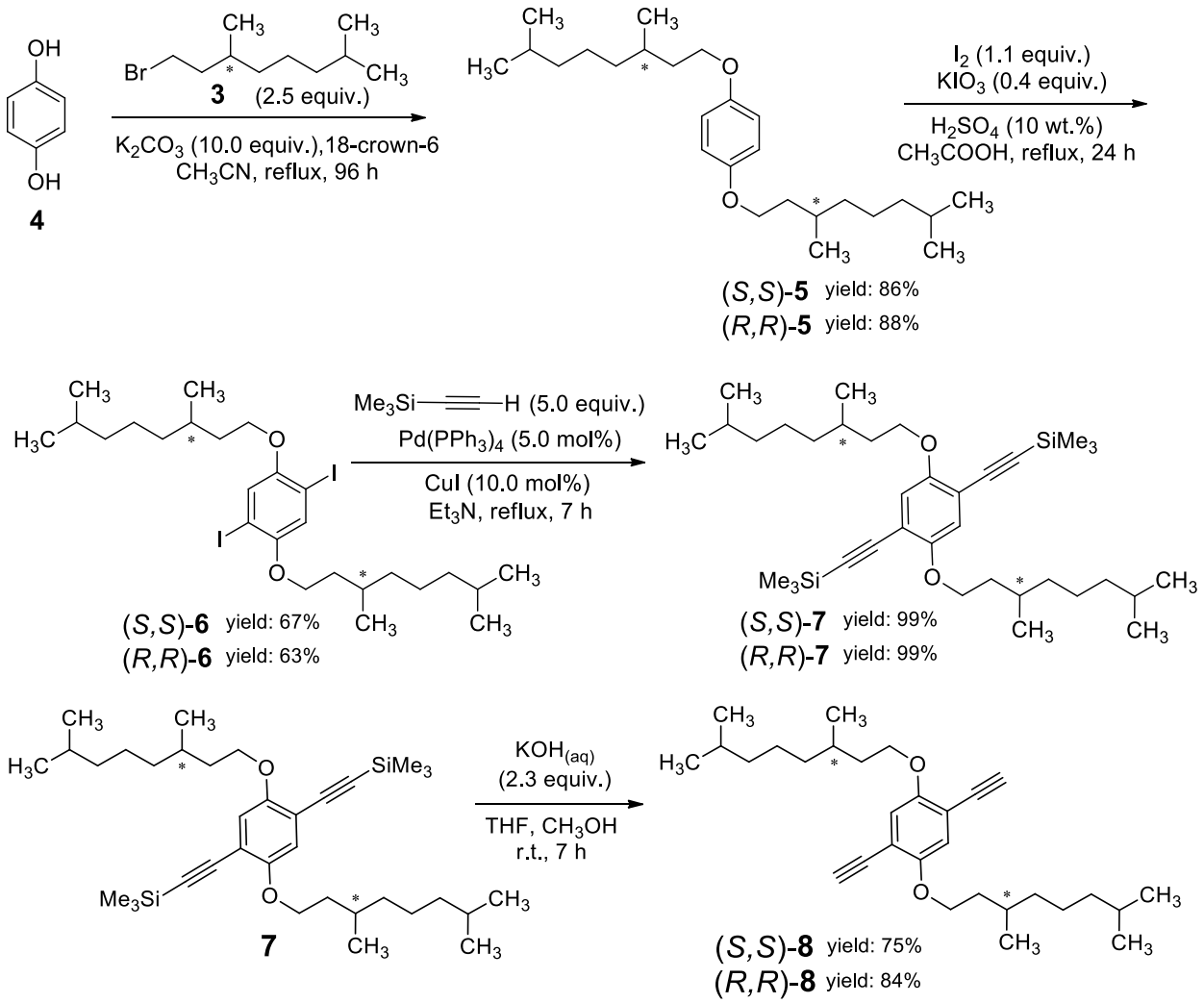


**Scheme S2**

**Synthesis of 1,4-bis(((*S*)-3,7-dimethyloctyl)oxy)benzene ((*S*,*S*)-5)** [S2]

Hydroquinone **4** (1.00 g, 9.1 mmol), (*S*)-1-bromo-3,7-dimethyloctane (*S*)-**3** (5.02 g, 22.7 mmol), $K_2CO_3$ (12.50 g, 90.4 mmol), 18-crown-6 (0.02 g, 0.08 mmol) were dissolved in $CH_3CN$ (100 mL). The mixture was refluxed under stirring for 96 h, then it was cooled to room temperature and concentrated under vacuum. The residue was hydrolyzed with $H_2O$ and extracted with $CH_2Cl_2$. The organic phase was washed with brine, dried over anhydrous $Na_2SO_4$ and the solvent was removed under vacuum. The crude product was purified through column chromatography ($SiO_2$, *n*-hexane → $CH_2Cl_2$) to give 1,4-bis(((*S*)-3,7-dimethyloctyl)oxy)benzene (*S*,*S*)-**5** (3.08 g, yield 86%) as a colourless oil.

$^1$H-NMR (400 MHz, $CDCl_3$), δ (ppm): 0.88 (12H, d, $J$ = 6.6 Hz), 0.94 (6H, d, $J$ = 6.6 Hz), 1.12-1.38 (12H, m), 1.49-1.61 (4H, m), 1.63-1.71 (2H, m), 1.77-1.85 (2H, m), 3.90-3.99 (4H, m), 6.83 (4H, s). $^{13}$C-NMR (100 MHz, $CDCl_3$), δ (ppm): 19.82, 22.75, 22.85, 24.81, 28.12, 30.00, 36.51, 37.47, 39.40, 67.12, 115.55 (2C), 153.35.

**Synthesis of 1,4-bis(((*R*)-3,7-dimethyloctyl)oxy)benzene ((*R,R*)-5)**

According to the previous procedure, 1,4-bis(((*R*)-3,7-dimethyloctyl)oxy)benzene (*R,R*)-**5** (88% yield) was obtained starting from hydroquinone and (*R*)-1-bromo-3,7-dimethyloctane (*R*)-**3**.

**Synthesis of 1,4-bis(((S)-3,7-dimethyloctyl)oxy)-2,5-diiodobenzene ((*S,S*)-6)** [S2]

1,4-Bis(((S)-3,7-dimethyloctyl)oxy)benzene (*S,S*)-**5** (2.00 g, 5.1 mmol), $KIO_3$ (0.45 g, 2.1 mmol), $I_2$ (1.48 g, 5.8 mmol), 10 wt% $H_2SO_4$ (3.3 mL) and $CH_3COOH$ (33 mL) were mixed together. The mixture was refluxed under stirring for 24 h, then it was cooled to room temperature, treated with 20 wt% $Na_2S_2O_4$ (15 mL) and extracted with $CH_2Cl_2$. The organic phase was washed with brine, dried over anhydrous $Na_2SO_4$ and the solvent was removed under vacuum. The crude product was purified through column chromatography ($SiO_2$, n-hexane/$CH_2Cl_2$ 4:1) to give 1,4-bis(((*S*)-3,7-dimethyloctyl)oxy)-2,5-diiodobenzene (*S,S*)-**6** (2.20 g, yield 67%) as a colourless oil.

$^1$H-NMR (400 MHz, $CDCl_3$), δ (ppm): 0.89 (12H, d, *J* = 6.6 Hz), 0.96 (6H, d, *J* = 6.6 Hz), 1.15-1.22 (4H, m), 1.25-1.40 (8H, m), 1.48-1.64 (4H, m), 1.72-1.80 (2H, m), 1.82-1.90 (2H, m), 3.91-4.01 (4H, m), 7.18 (2H, s). $^{13}$C-NMR (100 MHz, $CDCl_3$), δ (ppm): 19.80, 22.73, 22.84, 24.75, 28.03, 29.79, 36.16, 37.27, 39.27, 68.67, 86.35, 122.72, 152.90.

**Synthesis of 1,4-bis(((*R*)-3,7-dimethyloctyl)oxy)-2,5-diiodobenzene ((*R,R*)-6)**

According to the previous procedure, 1,4-bis(((*R*)-3,7-dimethyloctyl)oxy)-2,5-diiodobenzene (*R,R*)-**6** (63% yield) was obtained starting from 1,4-bis(((*R*)-3,7-dimethyloctyl)oxy)benzene (*R,R*)-**5**.

**Synthesis of ((2,5-bis(((*S*)-3,7-dimethyloctyl)oxy)-1,4-phenylene)bis(ethyne-2,1-diyl))bis(trimethylsilane) ((*S,S*)-7)**[S3]

To a solution of 1,4-bis(((S)-3,7-dimethyloctyl)oxy)-2,5-diiodobenzene (*S,S*)-**6** (1.00 g, 1.58 mmol) in $Et_3N$ (15 mL) were added 0.07 g (0.06 mmol) of $Pd(PPh_3)_4$, 0.03 g (0.16 mmol) of CuI and 1,1 mL (7.7 mmol) of trimethylsilylacetylene. The mixture was refluxed under stirring for 5h, at room temperature for 2h and then hydrolyzed with $NH_4Cl_{(aq)}$ and extracted with $CH_2Cl_2$. The organic phase was washed with brine, dried over anhydrous $Na_2SO_4$ and the solvent was removed under vacuum. The crude product was dissolved in pentane, filtered and the organic solution concentrated at reduced pressure, affording ((2,5-bis(((S)-3,7-

dimethyloctyl)oxy)-1,4-phenylene)bis(ethyne-2,1-diyl))bis(trimethylsilane) (*S*,*S*)-**7** (0.91 g, yield 99%) as an orange oil.

$^{1}$H-NMR (400 MHz, $CDCl_3$), δ (ppm): 0.25 (18H, s), 0.87 (12H, d, *J* = 6.7 Hz), 0.95 (6H, d, *J* = 6.6 Hz); 1.11-1.20 (6H, m), 1.26-1.37 (6H, m), 1.48-1.62 (4H, m), 1.71-1.79 (2H, m), 1.80-1.88 (2H, m), 3.94-4.02 (4H, m), 6.90 (2H, s). $^{13}$C-NMR (100 MHz, $CDCl_3$), δ (ppm): -0.06 (3C), 19.65, 22.56, 22.68, 24.72, 27.95, 29.76, 36.26, 37.34, 39.29, 67.72, 99.98, 101.08, 113.92, 117.16, 153.99. LC-MS (APCI$^+$), *m*/*z*: 583.61 $[M+H]^+$. Anal. calcd for $C_{36}H_{62}O_2Si_2$: C, 74.16; H, 10.72; found: C, 74.29; H, 10.59.

**Synthesis of ((2,5-bis(((*R*)-3,7-dimethyloctyl)oxy)-1,4-phenylene)bis(ethyne-2,1-diyl))bis(trimethylsilane) ((*R*,*R*)-7)**

According to the previous procedure, ((2,5-bis(((*R*)-3,7-dimethyloctyl)oxy)-1,4-phenylene)bis(ethyne-2,1-diyl))bis(trimethylsilane) (*R*,*R*)-**7** (99% yield) was obtained starting from 1,4-bis(((*R*)-3,7-dimethyloctyl)oxy)-2,5-diiodobenzene (*R*,*R*)-**6**.

**Synthesis of 1,4-bis(((S)-3,7-dimethyloctyl)oxy)-2,5-diethynylbenzene ((*S*,*S*)-8)[S3]**

A solution of ((2,5-bis(((*S*)-3,7-dimethyloctyl)oxy)-1,4-phenylene)bis(ethyne-2,1-diyl))bis(trimethylsilane) (*S*,*S*)-**7** (0.91 g, 1.57 mmol) in 67.5 mL of THF, 22.5 mL of methanol and 1.2 mL of KOH(aq) 3M was maintained under stirring at room temperature for 7h, then hydrolyzed with water and extracted with $CH_2Cl_2$.The organic phase was washed with brine, dried over anhydrous $Na_2SO_4$ and the solvent was removed under reduced pressure. The crude product was purified through column chromatography ($SiO_2$, petroleum ether /$CH_2Cl_2$ 8:2) to give 1,4-bis(((*S*)-3,7-dimethyloctyl)oxy)-2,5-diethynylbenzene (*S*,*S*)-**8** (0.52 g, 75% yield) as an orange oil.

$^{1}$H-NMR (400 MHz, $CDCl_3$), δ (ppm): 0.86 (12H, d, *J* = 6.7 Hz), 0.94 (6H, d, *J* = 6.7 Hz), 1.11-1.24 (6H, m), 1.25-1.37 (6H, m), 1.48-1.64 (4H, m), 1.64-1.76 (2H, m), 1.81-1.89 (2H, m), 3.32 (2H, s), 3.96-4.05 (4H, m), 6.96 (2H, s). $^{13}$C-NMR (100 MHz, $CDCl_3$), δ (ppm): 19.70, 22.59, 22.68, 24.65, 27.95, 29.80, 36.02, 37.23, 39.18, 67.97, 79.79, 82.40, 113.20, 117.60, 153.97. LC-MS (APCI$^+$), *m*/*z*: 439.57 $[M+H]^+$. Anal. calcd for $C_{30}H_{46}O_2$: C, 82.14; H, 10.57; found: C, 82.19; H, 10.63.

**Synthesis of 1,4-bis(((*R*)-3,7-dimethyloctyl)oxy)-2,5-diethynylbenzene ((*R*,*R*)-8)**

According to the previous procedure, 1,4-bis(((*R*)-3,7-dimethyloctyl)oxy)-2,5-diethynylbenzene (*R*,*R*)-**8** (84% yield) was obtained starting from ((2,5-bis(((*R*)-3,7-dimethyloctyl)oxy)-1,4-phenylene)bis(ethyne-2,1-diyl))bis(trimethylsilane) (*R*,*R*)-**7**.

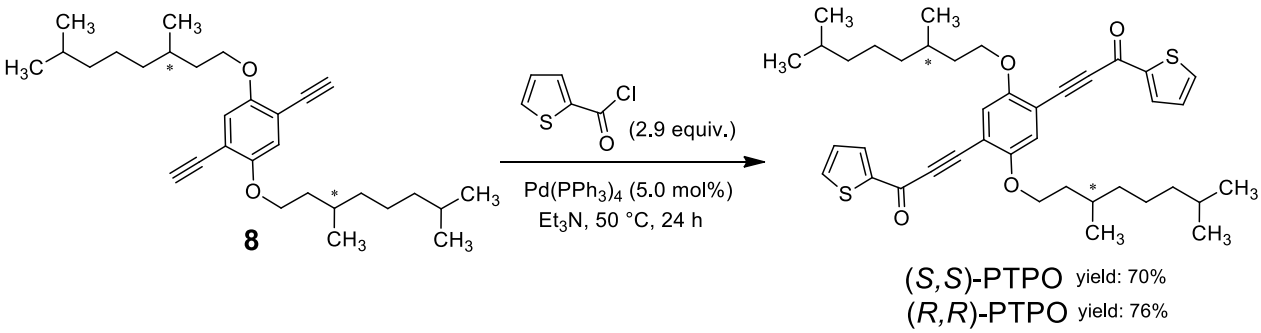


**Scheme S3**

**Synthesis of 3,3'-(2,5-bis(((*S*)-3,7-dimethyloctyl)oxy)-1,4-phenylene)bis(1-(thiophen-2-yl)prop-2-yn-1-one) ((*S*,*S*)-PTPO)[S3]**

1,4-Bis((*S*)-3,7-dimethyloctyloxy)-2,5-diethynylbenzene (*S*,*S*)-**8** (150 mg, 0.34 mmol), thiophene-2-carbonyl chloride (145 mg, 0.99 mmol), $Pd(PPh_3)_4$ (20 mg, 0.017 mmol) and $Et_3N$ (15 mL) were mixed together. The resulting mixture was left under stirring for 24 h at 50 °C, then it was cooled to room temperature, hydrolyzed with saturated ammonium chloride solution (20 mL) and extracted with $CH_2Cl_2$ (3×30 mL). The combined organic phases were washed with brine (50 mL), dried over anhydrous $Na_2SO_4$ and the solvent was removed under vacuum. The crude product was purified by column chromatography ($SiO_2$, *n*-hexane/$CH_2Cl_2$ 1:1) to give 3,3'-(2,5-bis((*S*)-3,7-dimethyloctyloxy)-1,4-phenylene)bis(1-(thiophen-2-yl)prop-2-yn-1-one) (*S*,*S*)-PTPO (157 mg, yield 70%) as a yellow solid.

$^1$H-NMR (400 MHz, $CDCl_3$), δ (ppm): 0.84 (12H, d, *J* = 6.6 Hz), 0.97 (6H, d, *J* = 6.6 Hz), 1.12-1.25 (6H, m), 1.28-1.38 (6H, m), 1.45-1.55 (2H, m), 1.68-1.78 (4H, m), 1.91-1.99 (2H, m), 4.04-4.13 (4H, m), 7.15-7.18 (4H, m), 7.74 (2H, dd, *J* = 4.9, 1.3 Hz), 8.15 (2H, dd, *J* = 3.8, 1.3 Hz). $^{13}$C-NMR (100 MHz, $CDCl_3$), δ (ppm): 19.51, 22.51, 22.63, 24.57, 27.88, 29.74, 36.22, 37.19, 39.15, 67.84, 87.71, 92.11, 112.93, 117.43, 128.11, 135.36, 136.12, 145.04, 154.91, 169.60. LC-MS (APCI$^+$), *m*/*z*: 659.31[M+H]$^+$. Anal. calcd for $C_{40}H_{50}O_4S_2$: C, 72.91; H, 7.65; S, 9.73; found: C, 72.84; H, 7.69; S, 9.72.

**Synthesis of 3,3'-(2,5-bis(((*R*)-3,7-dimethyloctyl)oxy)-1,4-phenylene)bis(1-(thiophen-2-yl)prop-2-yn-1-one) ((*R*,*R*)-PTPO)**

According to the previous procedure, 3,3'-(2,5-bis(((*R*)-3,7-dimethyloctyl)oxy)-1,4-phenylene)bis(1-(thiophen-2-yl)prop-2-yn-1-one) (*R*,*R*)-PTPO (76% yield) was obtained starting from 1,4-bis(((*R*)-3,7-dimethyloctyl)oxy)-2,5-diethynylbenzene (*R*,*R*)-**8**.

## Thin film preparation

The films were prepared by spin-coating (Laurell WS-650MZ-23NPPB) 100 μL of a $4 \cdot 10^{-2}$ M solution of PTPO in $CH_2Cl_2$ onto a 25x25 $mm^2$ glass substrate. Spin coating conditions: 2000 rpm, 30 sec, acceleration 1000 rpm/sec. The films were then thermally annealed in an oven at 80 °C for 1 hour.

## Thin film optimization

Spin-coating parameters were optimized recording CP emission and ECD spectra as a function of film thickness. Figure S1 shows a maximum of both $|g_{abs}|$ and $|g_{lum}|$ values for absorbance around 0.35-0.4, corresponding to 300 nm thickness.

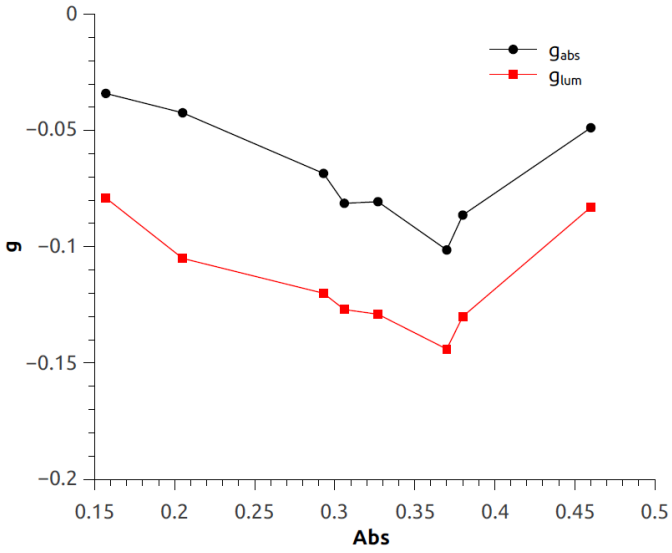


**Figure S1.** $g_{abs}$ (black) and $g_{lum}$ (red) values as a function of absorbance (465 nm) for thermally annealed (*S*,*S*)-PTPO films measured in forward configuration.

## Thin film pictures

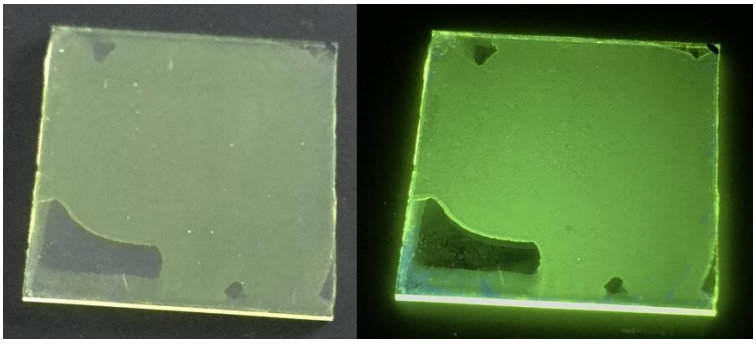

**Figure S2.** Picture of a (*S*,*S*)-PTPO thin film under ambient (left) and 365 nm UV light (right) illumination.

## ECD and CP emission spectra measurements

ECD spectra were measured with a Jasco J-715 spectropolarimeter. CP emission spectra were measured with a home-made spectrofluoropolarimeter[S4] (see Figure S3). The samples were excited with a 365 nm LED source with 0° geometry achieved by means of a dichroic mirror (TECHSPEC®, reflection band 350-375 nm, transmission band 420-1600 nm). The following acquisition parameters were employed: slit-width 5 nm, scan-speed 1 nm/sec, integration time 1 sec, PMT HV 600 V, PEM modulation 50 KHz.

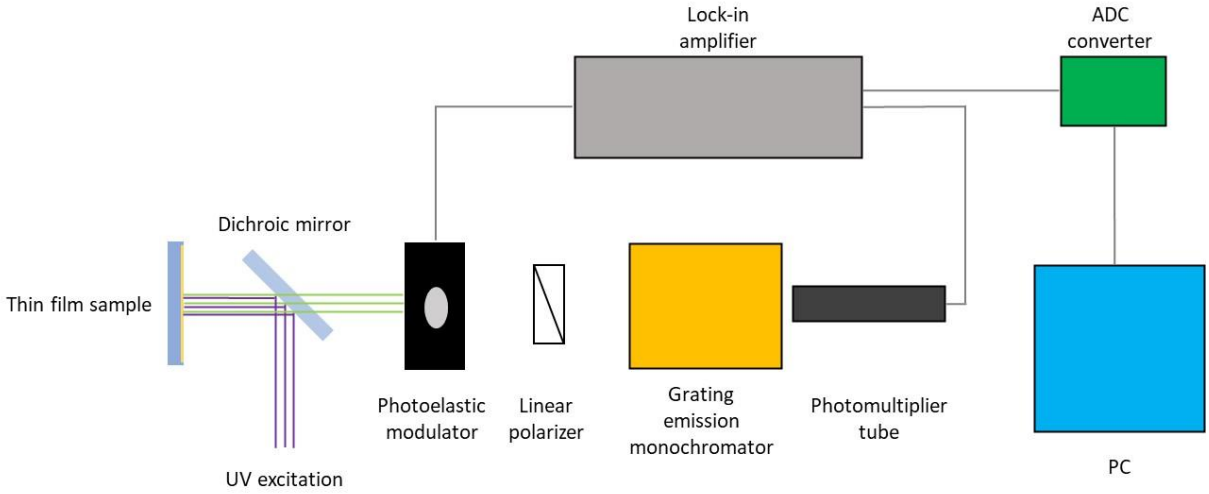


**Figure S3.** Experimental set-up employed for CP emission measurements.

Residual fluorescence linear anisotropy was measured using lock-in detection at double frequency (100 KHz) with respect to the PEM modulation frequency and it is plotted as $P = \frac{I_{\parallel}-I_{\perp}}{I_{\parallel}+I_{\perp}}$, with $I_{\parallel}$ and $I_{\perp}$ being linearly polarized orthogonal components in emission.

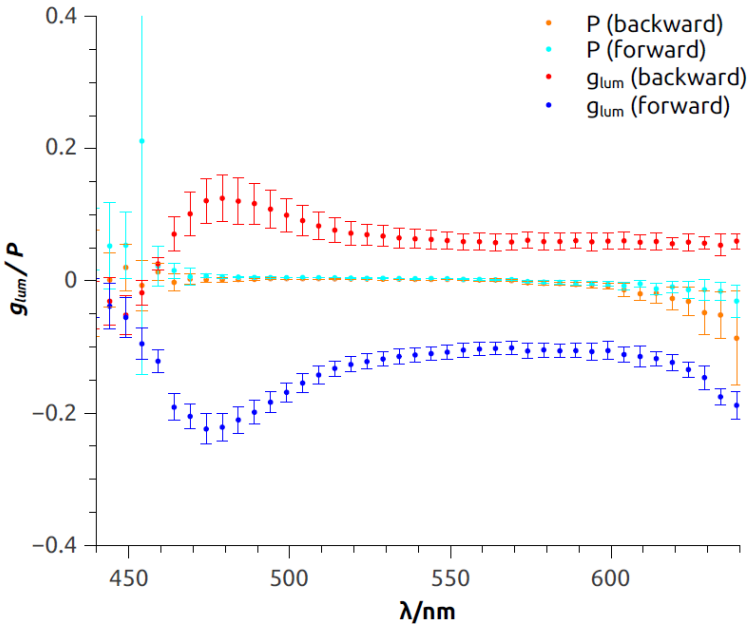


**Figure S4.** Residual linear polarization *P* for (*S*,*S*)-PTPO thin films in forward and backward configuration compared with $g_{lum}$ values.

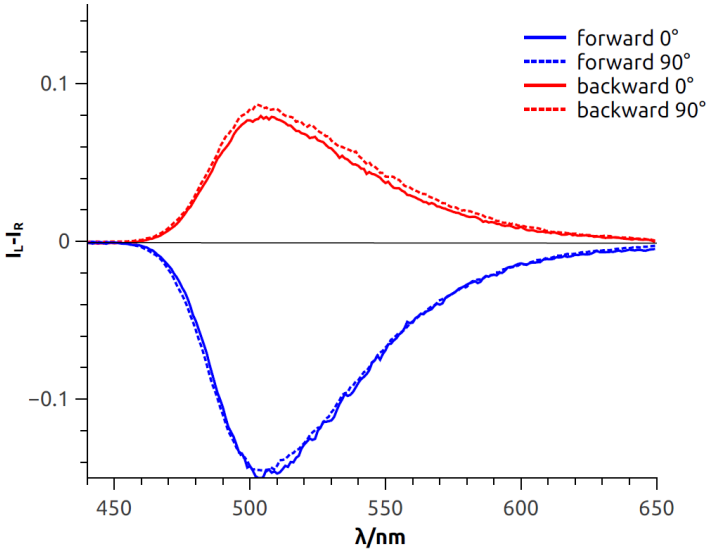


**Figure S5.** CP emission measured for a (*S*,*S*)-PTPO thin film by rotating the sample around its optical axis (0° and 90°) both in forward and backward configuration.

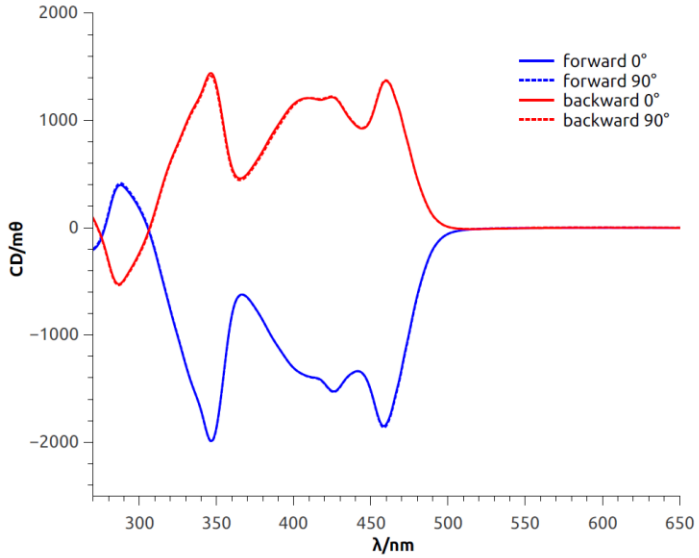


**Figure S6.** ECD spectra measured for a (*S*,*S*)-PTPO thin film by rotating the sample around its optical axis (0° and 90°) both in forward and backward configuration.

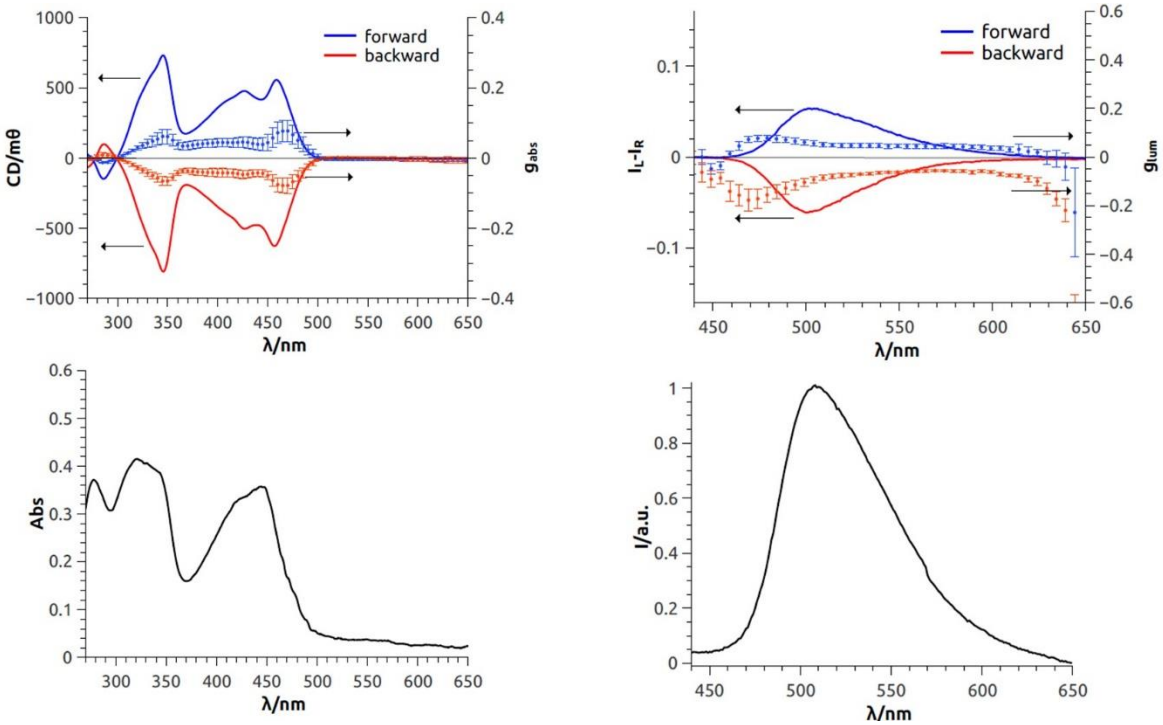


**Figure S7.** Left: ECD, $g_{abs}$ values and absorption spectrum of (*R*,*R*)-PTPO films in forward and backward configuration. Right: CP emission, $g_{lum}$ values and emission spectrum of the film in forward and backward configuration. The error bars on $g_{abs}$ and $g_{lum}$ values represent one standard deviation calculated over 5 replicates).

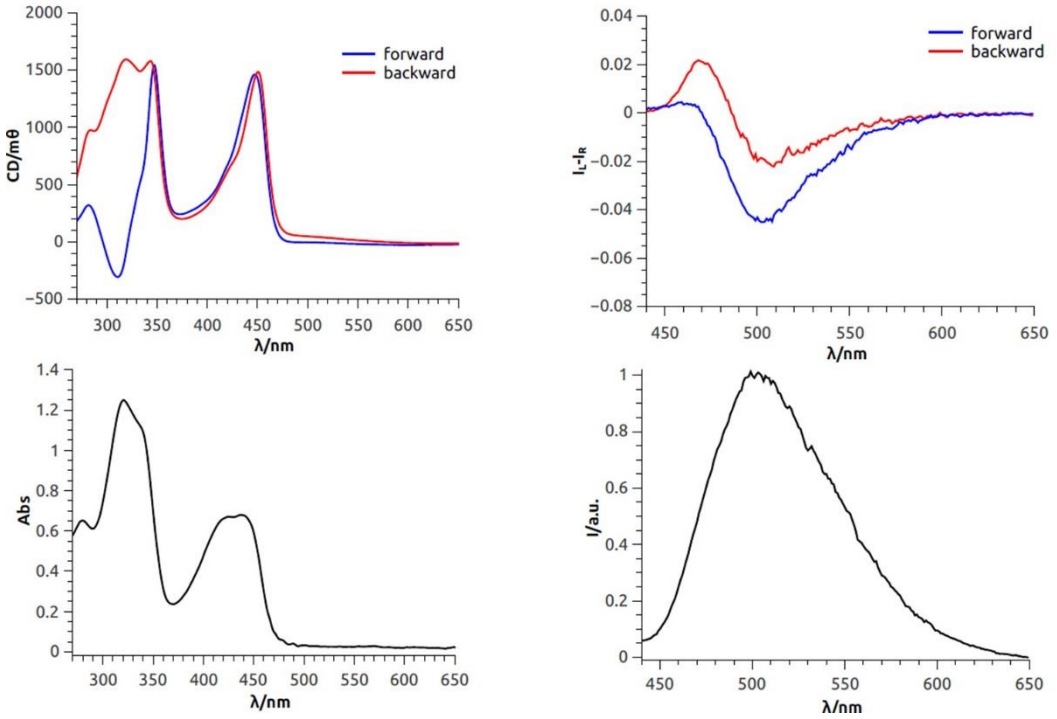


**Figure S8.** Left: ECD and absorption spectrum of (*S*,*S*)-PTPO films before thermal annealing in forward and backward configuration. Right: CP emission and emission spectrum of (*S*,*S*)-PTPO films before thermal annealing in forward and backward configuration.

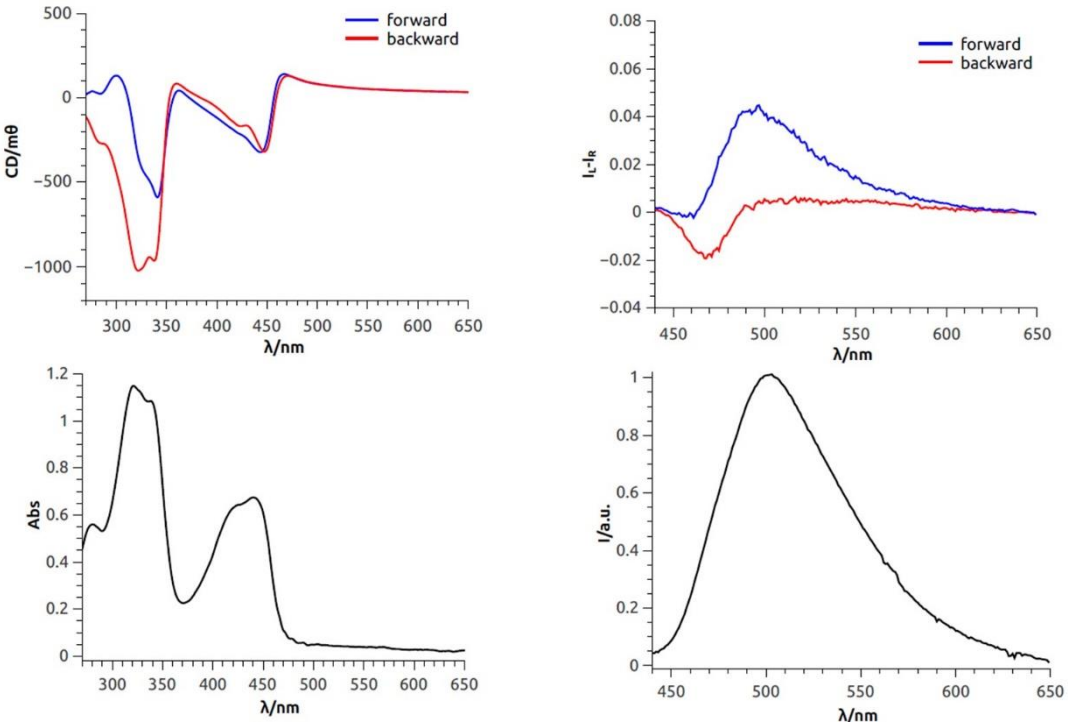


**Figure S9.** Left: ECD and absorption spectrum of (*R*,*R*)-PTPO films before thermal annealing in forward and backward configuration. Right: CP emission and emission spectrum of (*R*,*R*)-PTPO films before thermal annealing in forward and backward configuration.

## Optical microscopy images

FE-SEM images were acquired on a FEI Quanta 450 ESEM FEG instrument using secondary electron detection. The samples were coated with a 6 nm Pt layer. AFM images were recorded with a Veeco Instruments Inc. (USA), model NanoScope IIIa with MultiMode head, equipped with ADC5 extension, TAC temperature controller and gas cell. The AFM was combined to an external controller (PLLProII, RHK Technology, Troy, USA) for frequency modulation (FM) operation, based on a phase-locked loop (PLL) detector. The output of such detector is the instantaneous resonant frequency of the AFM sensor oscillation, $\Delta f(t)$. The scanning mode used was the FM-AFM at constant excitation, using oscillation amplitude for distance regulation. The use of this scanning mode allows quantitative estimation of surface dissipation. The used AFM sensors were high-resolution cantilever probes from MikroMasch (model Hi'Res-C14/Cr-Au, Chromium-Gold coated silicon with sharp diamond-like spike, nominal tip radius 1 nm, spring constant ~ 5 N/m, resonant frequency $f_0$ ~ 118.8 kHz, quality factor $Q_0$ ~ 300 in air). Used oscillation amplitude was around 15 nm. Measurements were performed at room temperature and in ambient atmosphere. Two perpendicular scratches on each film was made by gently dragging the tip of a steel cutter along the sample surface. Two different points of the film were imaged by AFM, close to each scratch. Fast scanning direction was always chosen as perpendicular to each scratch. Scanning speed was always kept below 2 mm/s, to preserve the probe tip.

Optical microscopy images were recorded with a Zeiss discovery V8 equipped with linearly polarizing filters.

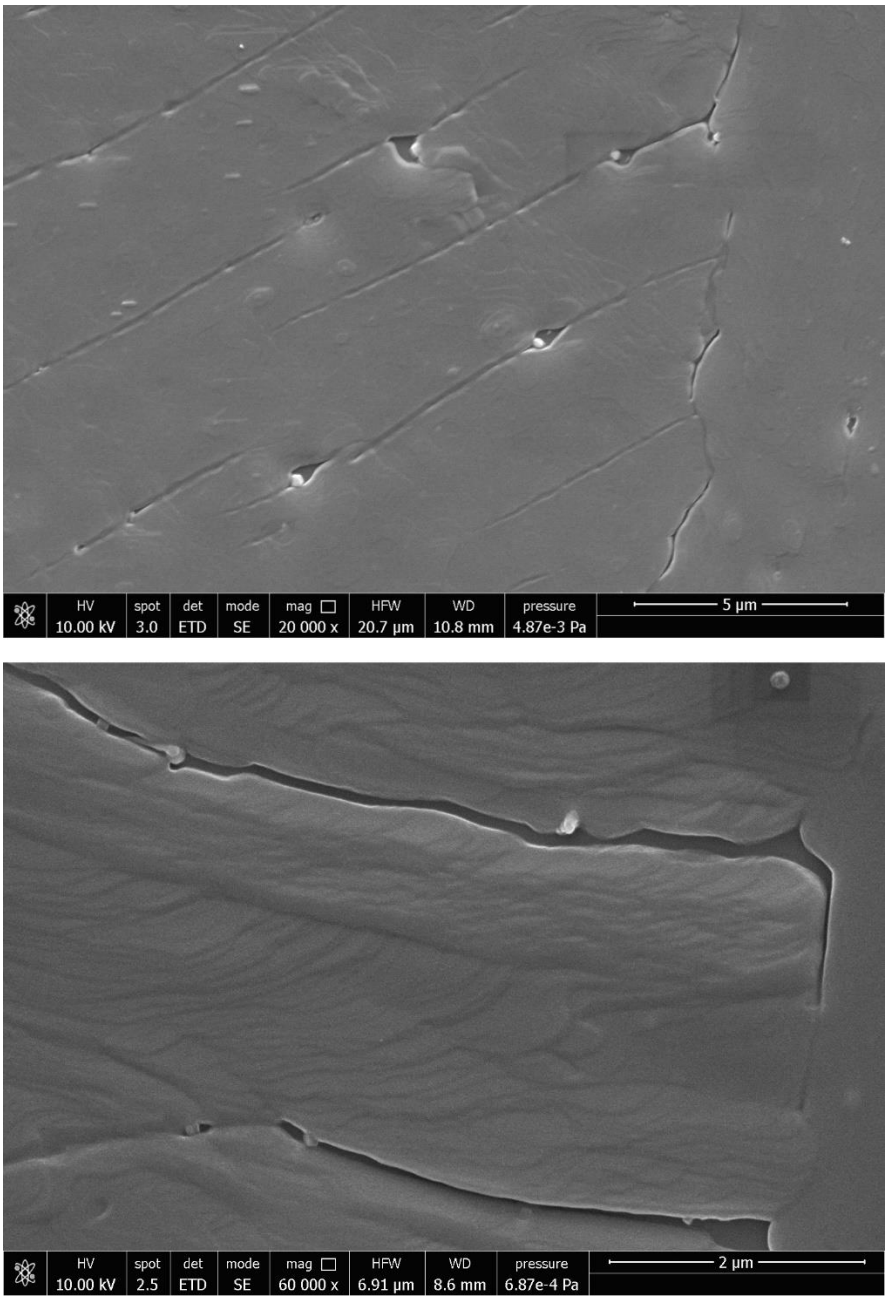


**Figure S10.** FE-SEM images of a thermally annealed thin film of (*S*,S)-PTPO.

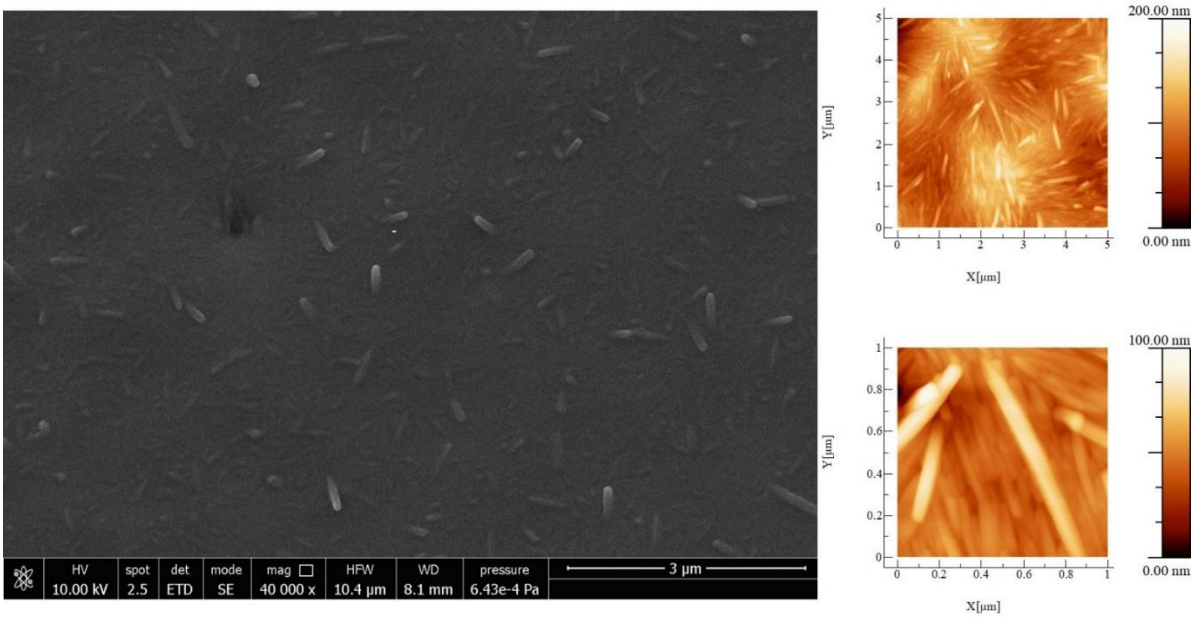


**Figure S11.** Left: FE-SEM image of a non-annealed thin film of (*S*,S)-PTPO. Right: AFM images of portions of the non-annealed thin film.

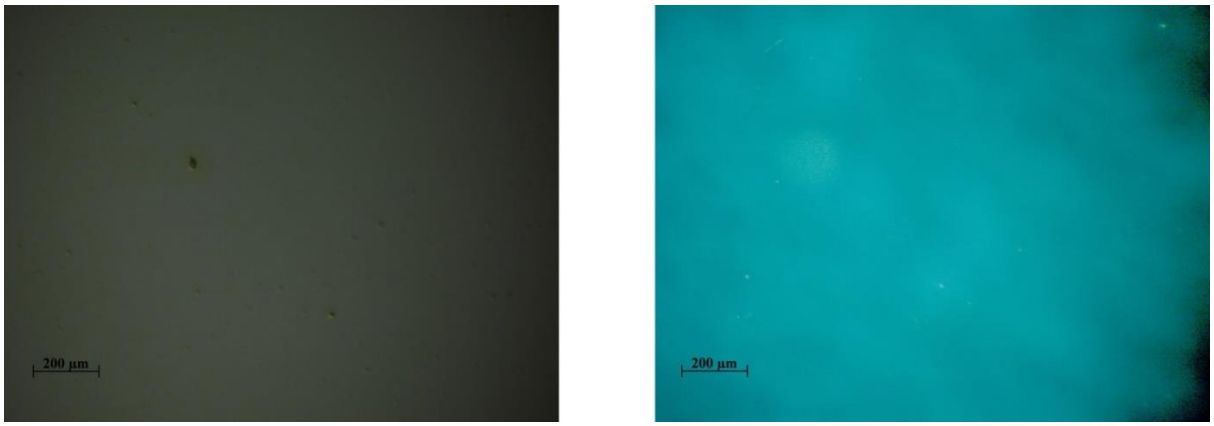


**Figure S12.** Bright field (left) and crossed polarized (right) optical microscopy images of a non-annealed (*S*,S)-PTPO thin film.

## Futuristic applications of non-reciprocal CP emitting materials in CP-OLEDs

One of the expected applications of emergently non-reciprocal CP emitting materials is their use in CP-OLEDs. In principle, when regular CP emitters are embedded in the active layer of a CP-OLED, polarized back-emitted light is partially reflected by the reflecting cathode with ensuing polarization handedness reversals and lower polarization efficiency of the device. On the other hand, new materials displaying non-reciprocal CP properties would be exempted from such detrimental effect, thanks to the fact that the backward component has an opposite CP with respect to the forward one. In this way, upon reflection, both the components will recover the same polarization, improving the total polarization output of the device (Figure S13).

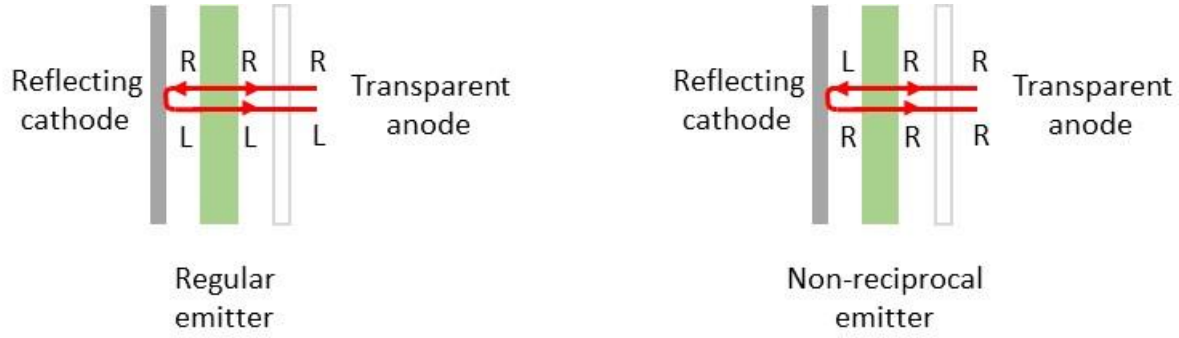


**Figure S13.** Fate of CP light inside an electronic device when emitted by a regular (left) and a non-reciprocal (right) material.

## $^{1}$H-NMR and $^{13}$C-NMR spectra of synthesized compounds

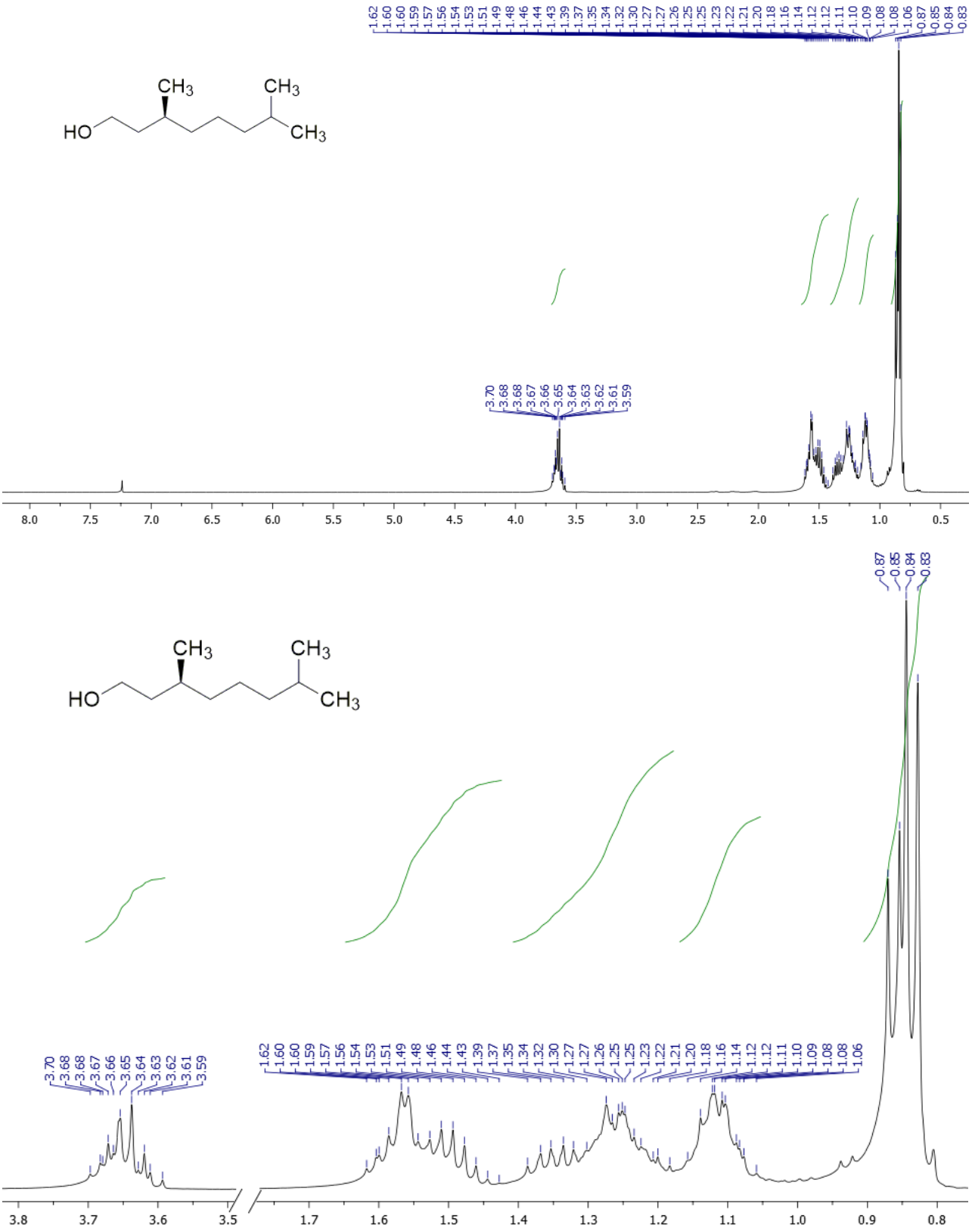


**Figure S14.** $^{1}$H-NMR spectrum (400 MHz, $CDCl_3$) of (*S*)-3,7-dimethyloctan-1-ol (*S*)-**2**: full scale spectrum (top) and spectrum expansions (bottom).

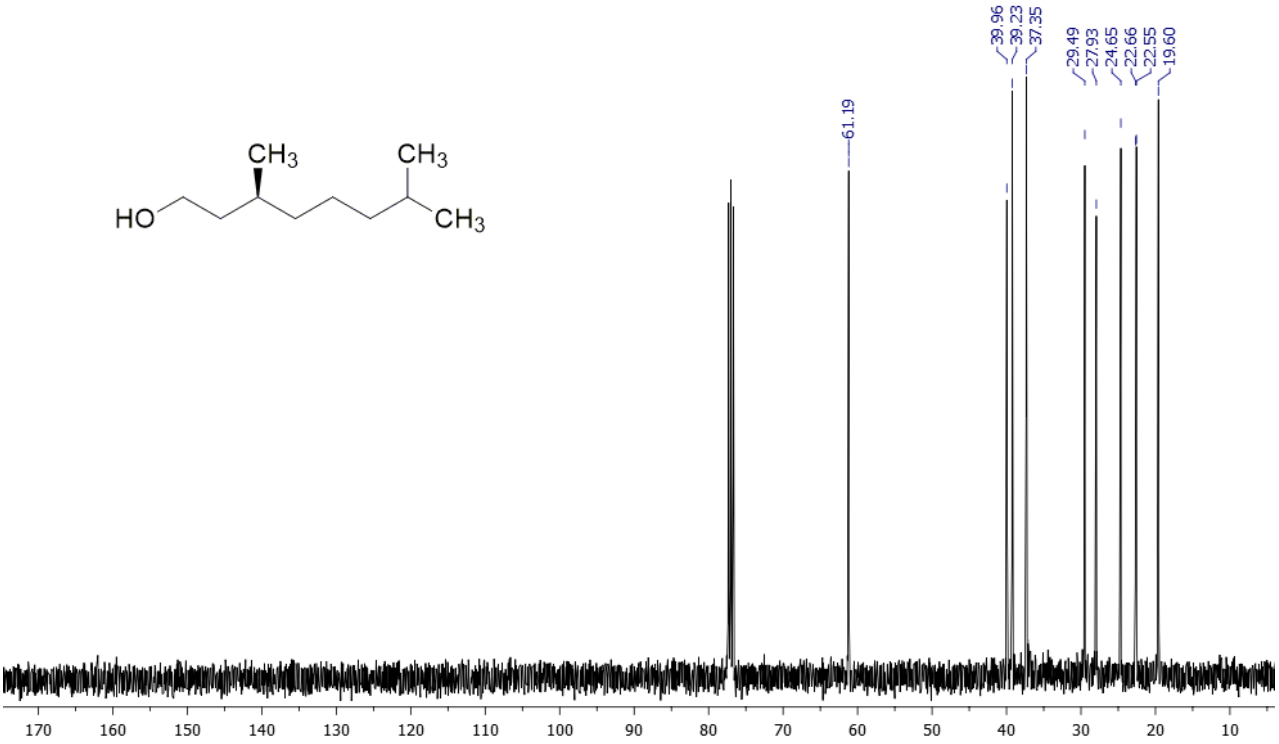


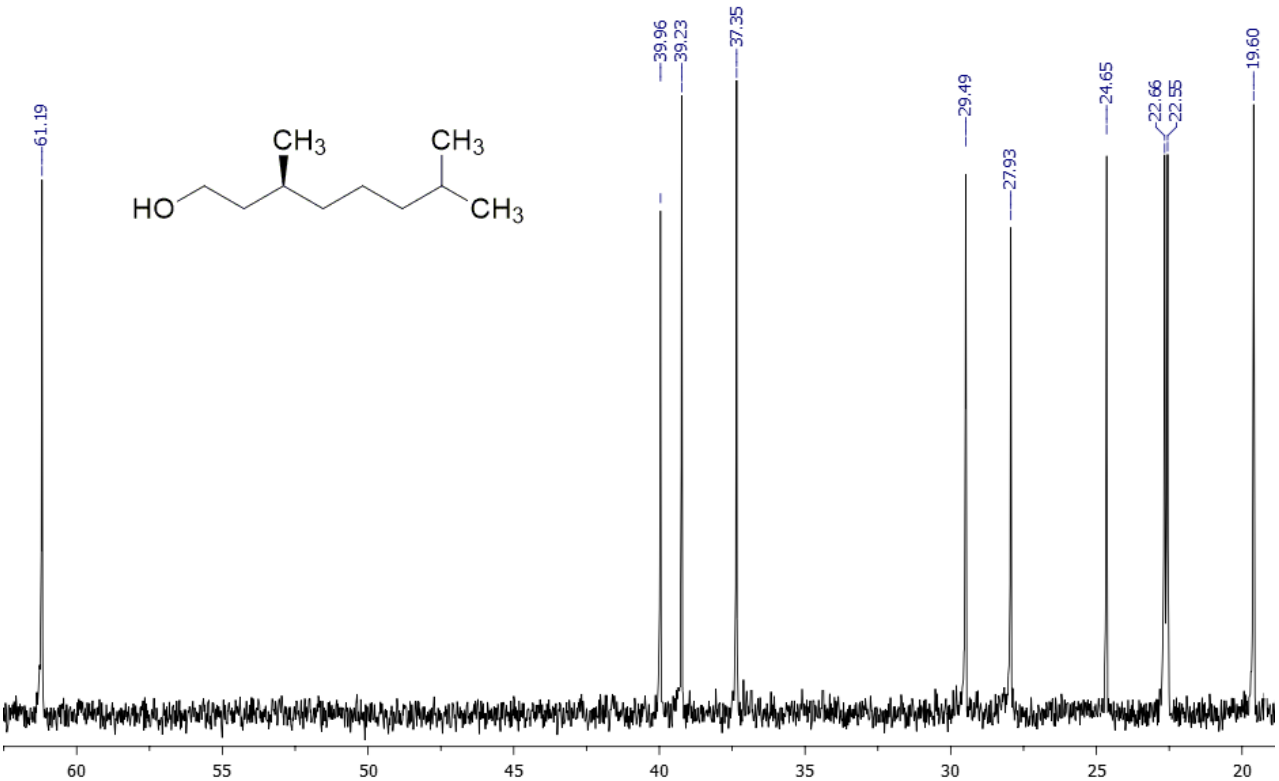


**Figure S15.** $^{13}$C-NMR spectrum (100 MHz, $CDCl_3$) of (*S*)-3,7-dimethyloctan-1-ol (*S*)-**2**: full scale spectrum (top) and spectrum expansions (bottom).

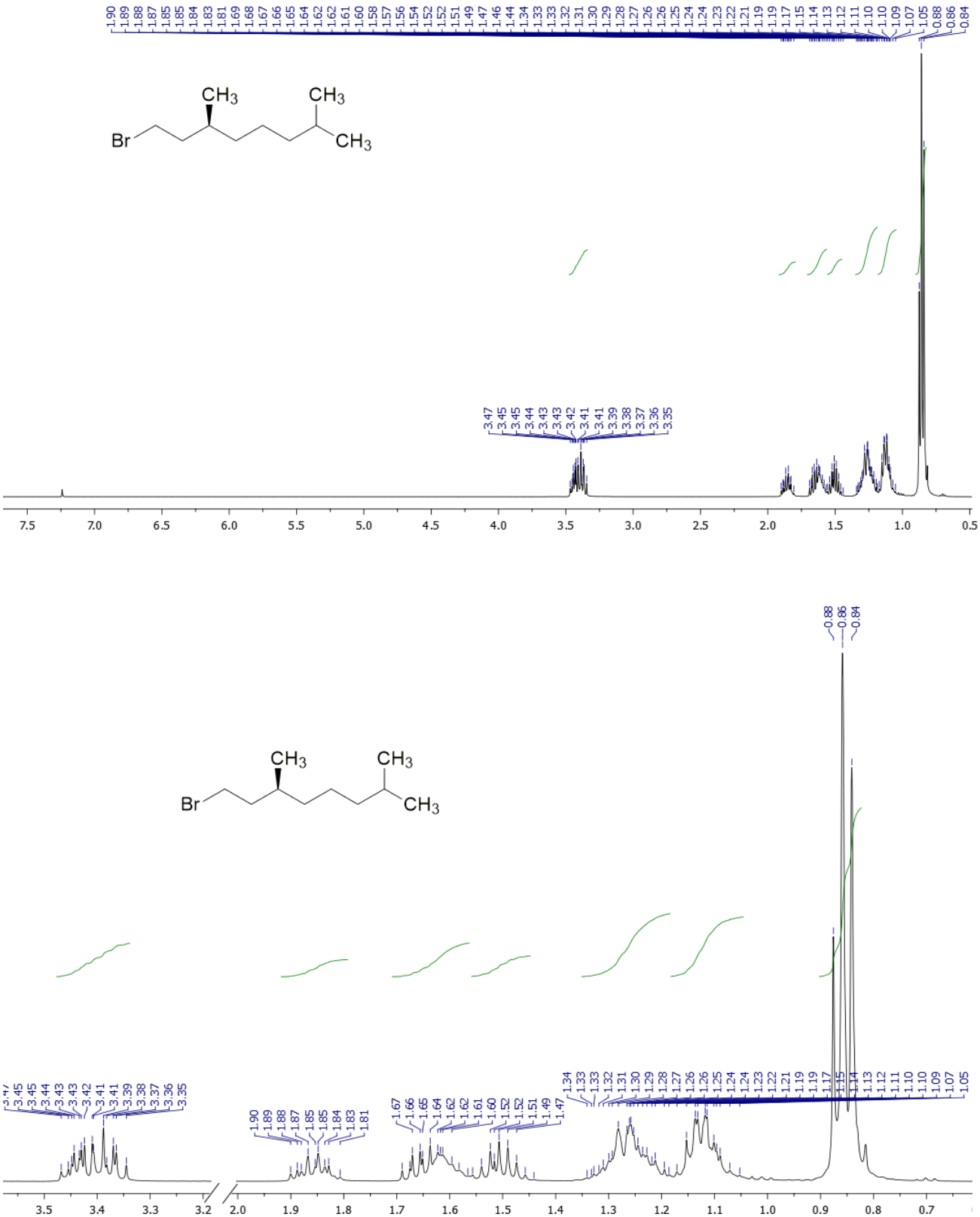


**Figure S16.** $^{1}$H-NMR spectrum (400 MHz, $CDCl_3$) of (*S*)-1-bromo-3,7-dimethyloctane (*S*)-**3**: full scale spectrum (top) and spectrum expansions (bottom).

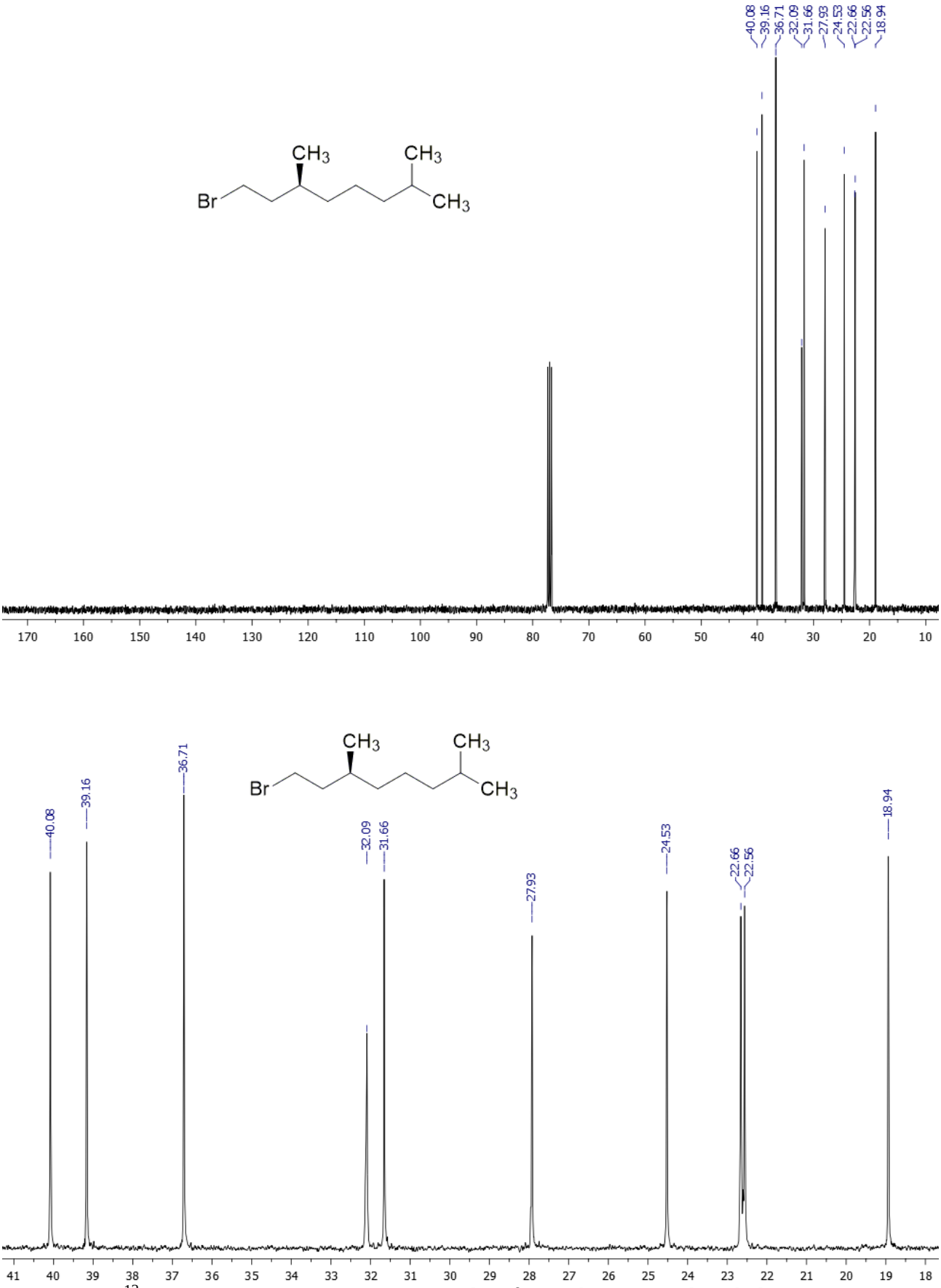


**Figure S17.** $^{13}$C-NMR spectrum (100 MHz, $CDCl_3$) of (*S*)-1-bromo-3,7-dimethyloctane (*S*)-**3**: full scale spectrum (top) and spectrum expansions (bottom).

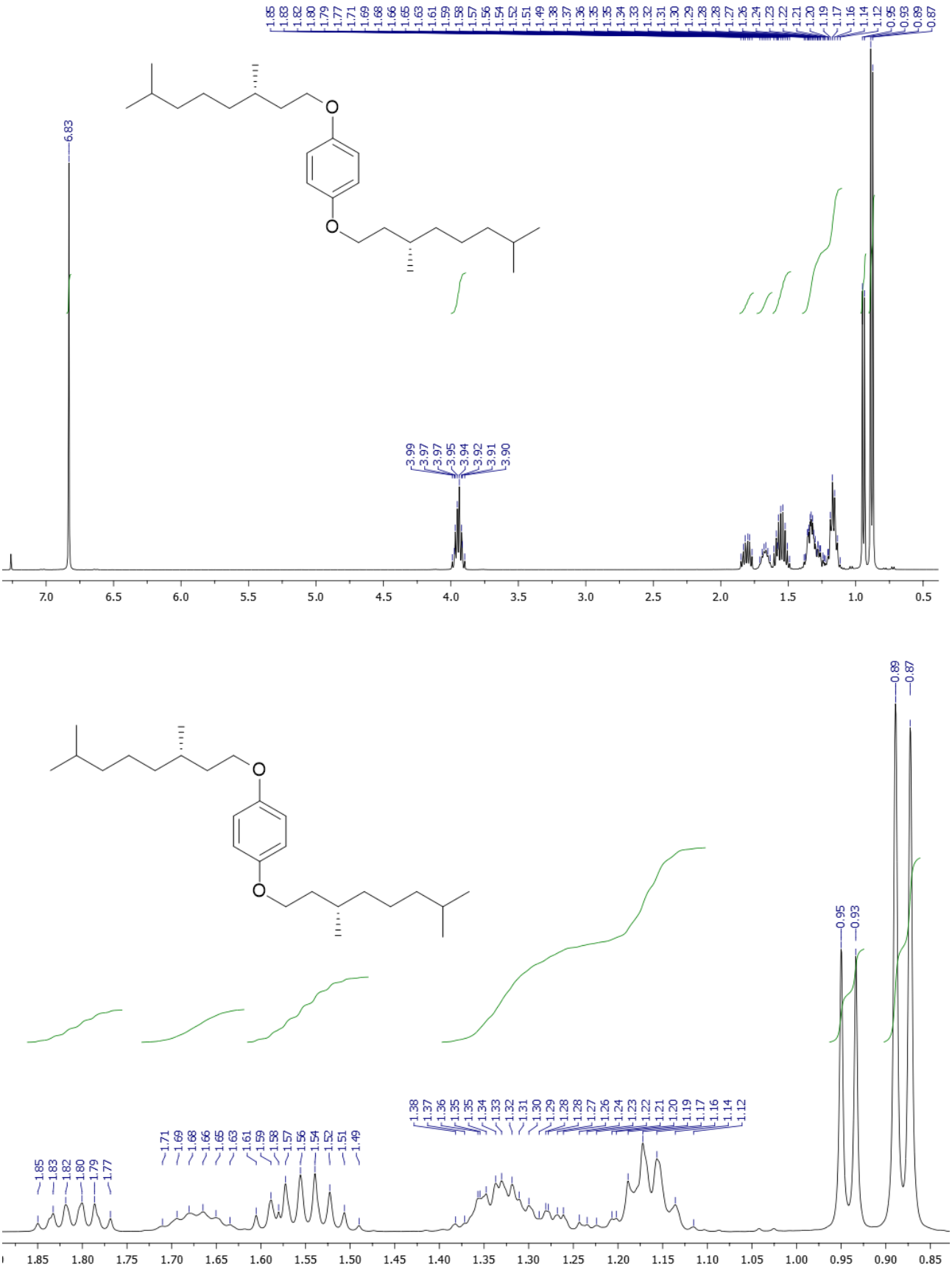

**Figure S18.** $^{1}$H-NMR spectrum (400 MHz, $CDCl_3$) of 1,4-bis(((*S*)-3,7-dimethyloctyl)oxy)benzene (*S*,*S*)-**5**: full scale spectrum (top) and spectrum expansions (bottom).

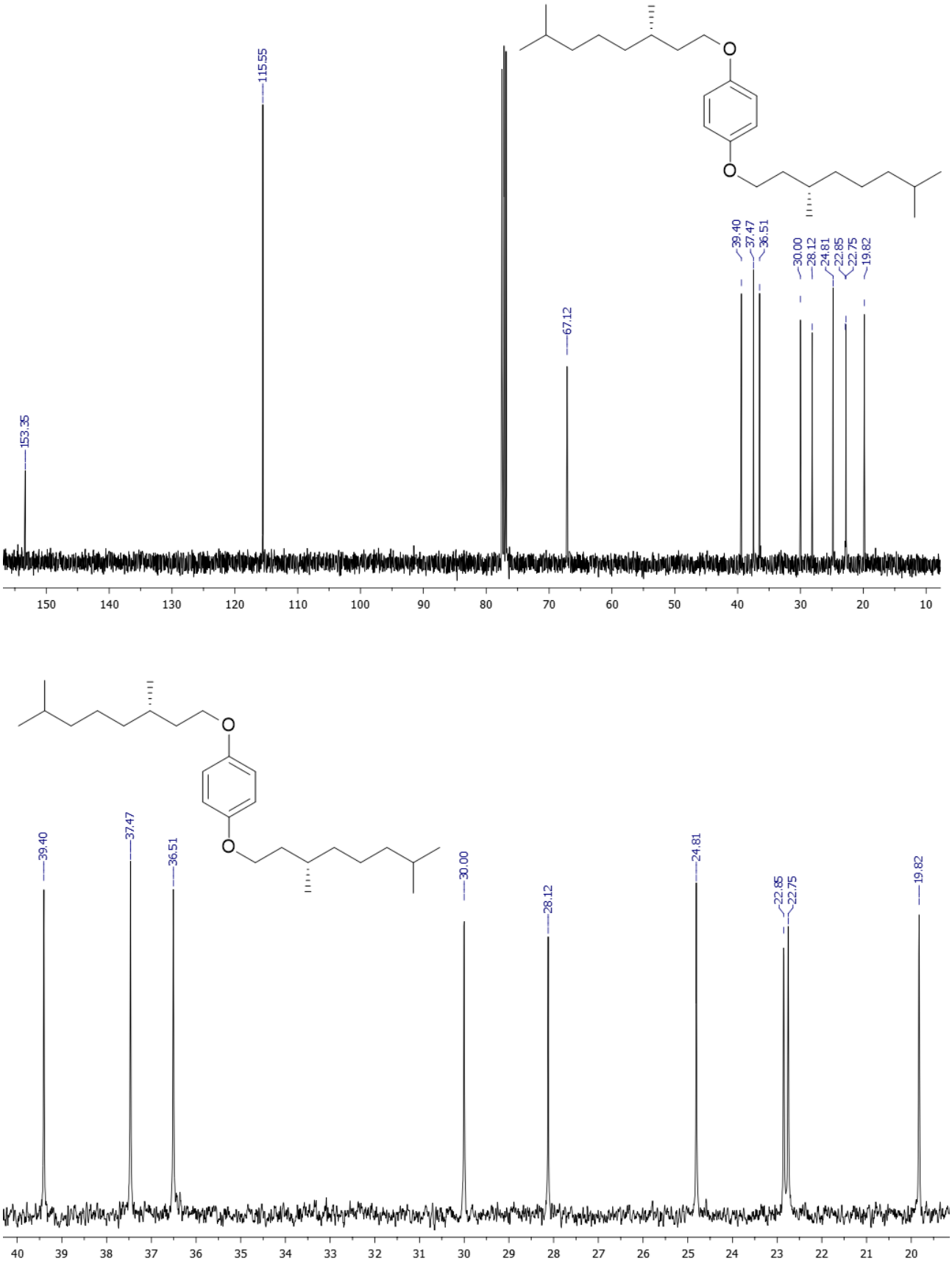


**Figure S19.** $^{13}$C-NMR spectrum (100 MHz, $CDCl_3$) of 1,4-bis(((*S*)-3,7-dimethyloctyl)oxy)benzene (*S*,*S*)-**5**: full scale spectrum (top) and spectrum expansions (bottom).

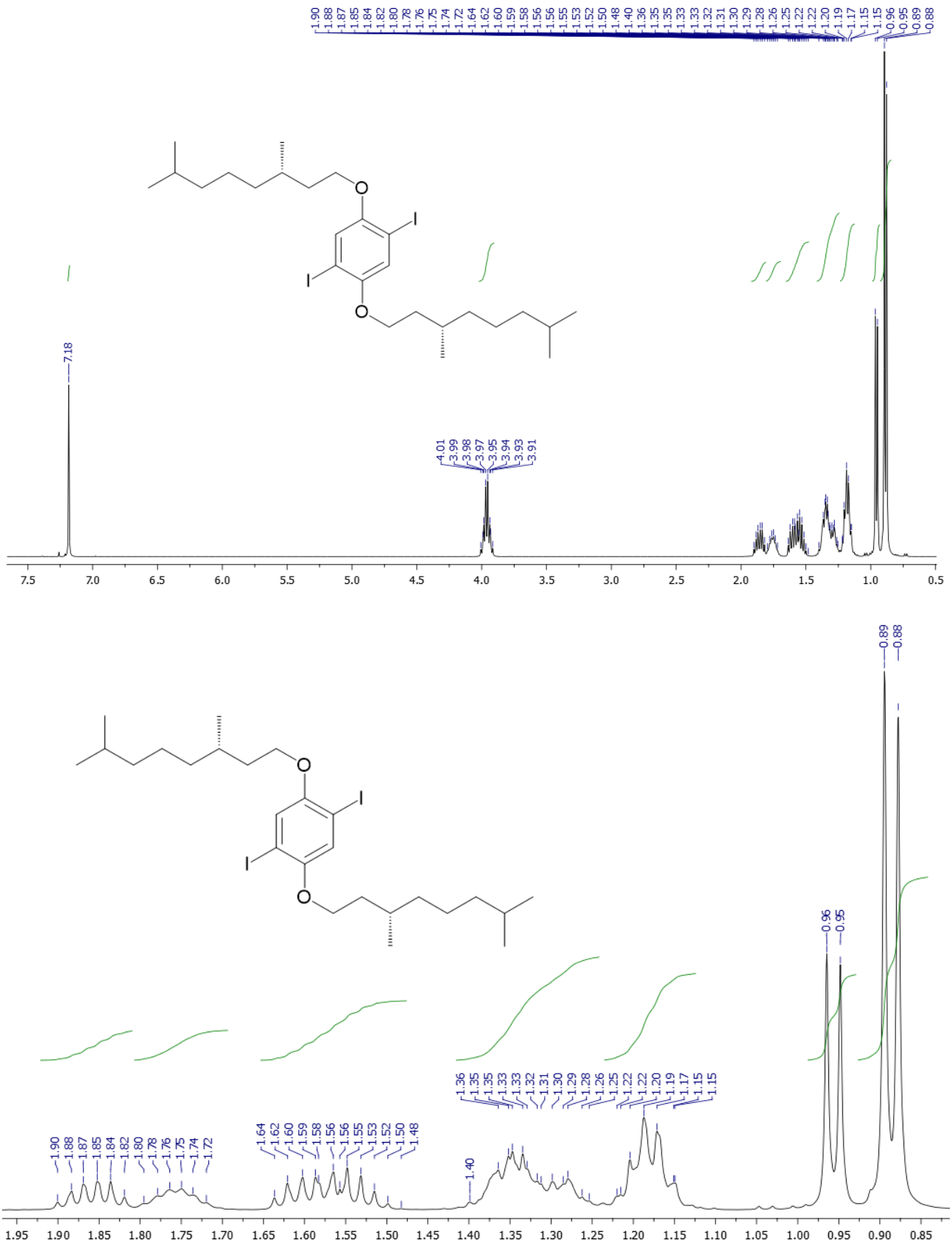

**Figure S20.** $^{1}$H-NMR spectrum (400 MHz, $CDCl_3$) of 1,4-bis(((*S*)-3,7-dimethyloctyl)oxy)-2,5-diiodobenzene (*S*,*S*)-**6**: full scale spectrum (top) and spectrum expansions (bottom).

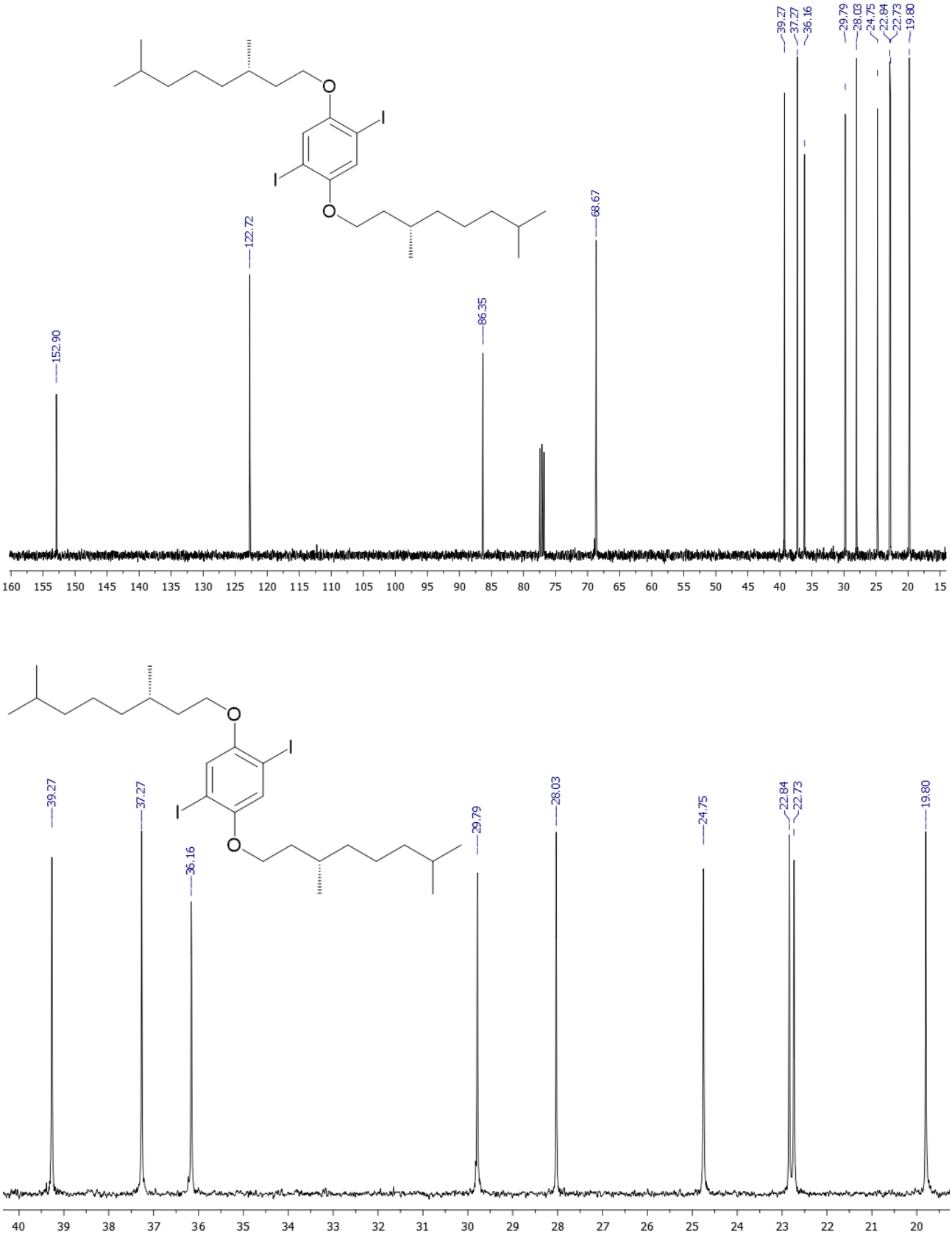


**Figure S21.** $^{13}$C-NMR spectrum (100 MHz, $CDCl_3$) of 1,4-bis(((*S*)-3,7-dimethyloctyl)oxy)-2,5-diiodobenzene (*S*,*S*)-**6**: full scale spectrum (top) and spectrum expansions (bottom).

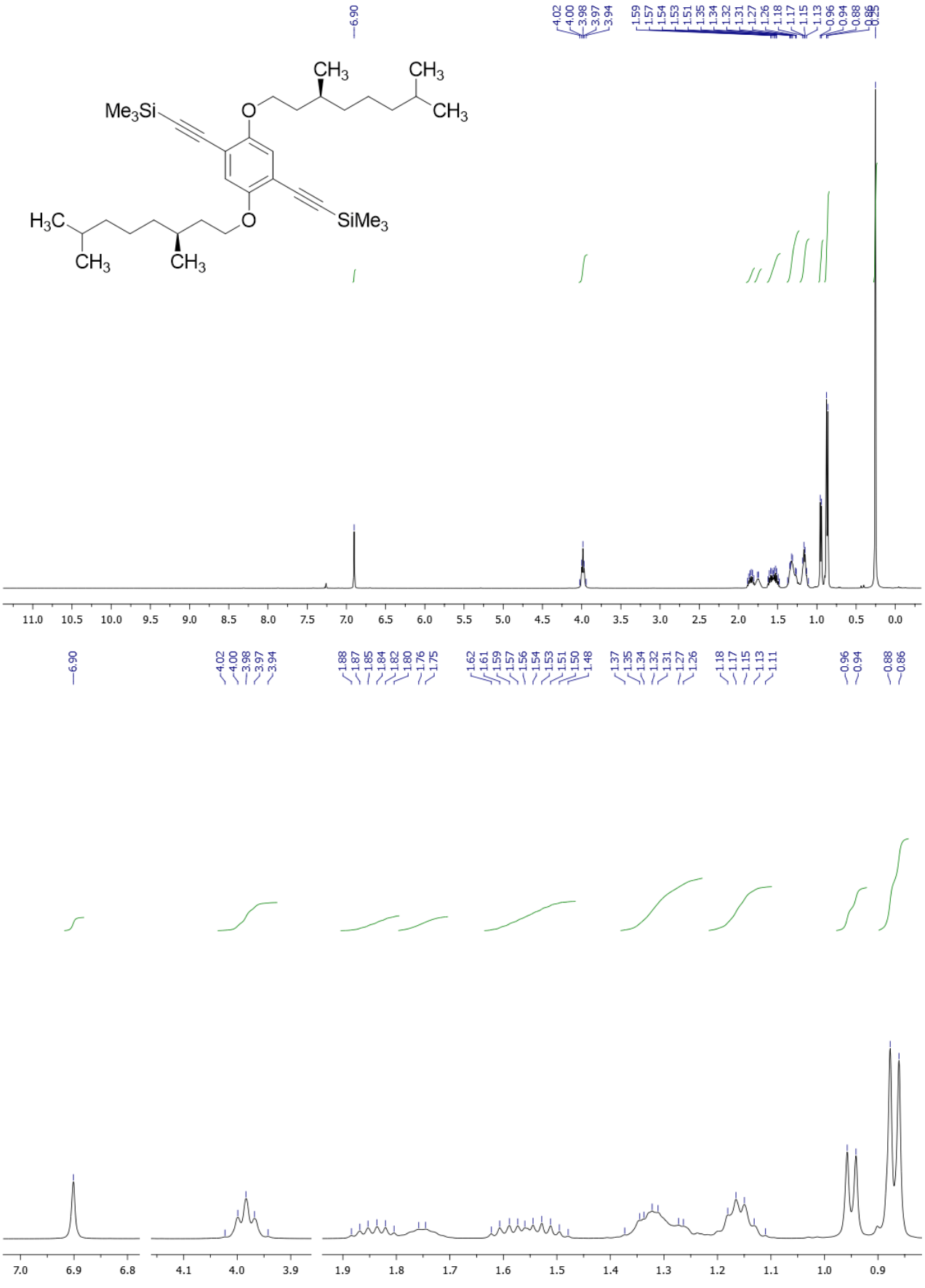
6.90
4.02
4.00
3.98
3.97
3.94
1.59
1.57
1.54
1.53
1.51
1.35
1.34
1.32
1.31
1.27
1.26
1.18
1.17
1.15
1.13
0.96
0.94
0.88
0.86
Me3Si
SiMe3
H3C
CH3
O
11.0
10.5
10.0
9.5
9.0
8.5
8.0
7.5
7.0
6.5
6.0
5.5
5.0
4.5
4.0
3.5
3.0
2.5
2.0
1.5
1.0
0.5
0.0
1.88
1.87
1.85
1.84
1.82
1.80
1.76
1.75
1.62
1.61
1.59
1.57
1.56
1.54
1.53
1.51
1.50
1.48
1.37
1.35
1.34
1.32
1.31
1.27
1.26
1.18
1.17
1.15
1.13
1.11
7.0
6.9
6.8
4.1
4.0
3.9
1.9
1.8
1.7
1.6
1.5
1.4
1.3
1.2
1.1
1.0
0.9

**Figure S22.** $^{1}$H-NMR spectrum (400 MHz, $CDCl_3$) of ((2,5-bis(((*S*)-3,7-dimethyloctyl)oxy)-1,4-phenylene)bis (ethyne-2,1-diyl))bis(trimethylsilane) (*S*,*S*)-**7**: full scale spectrum (top) and spectrum expansions (bottom).

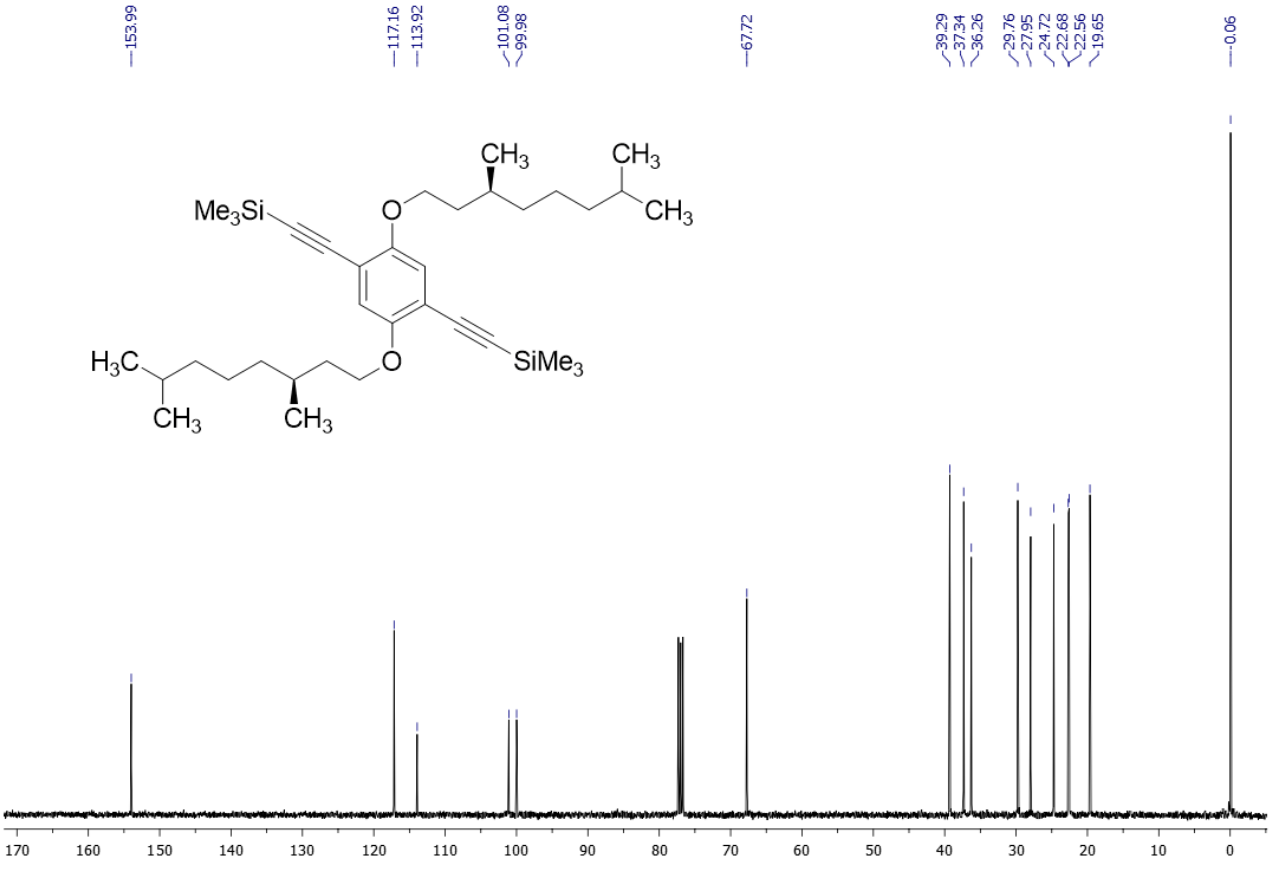

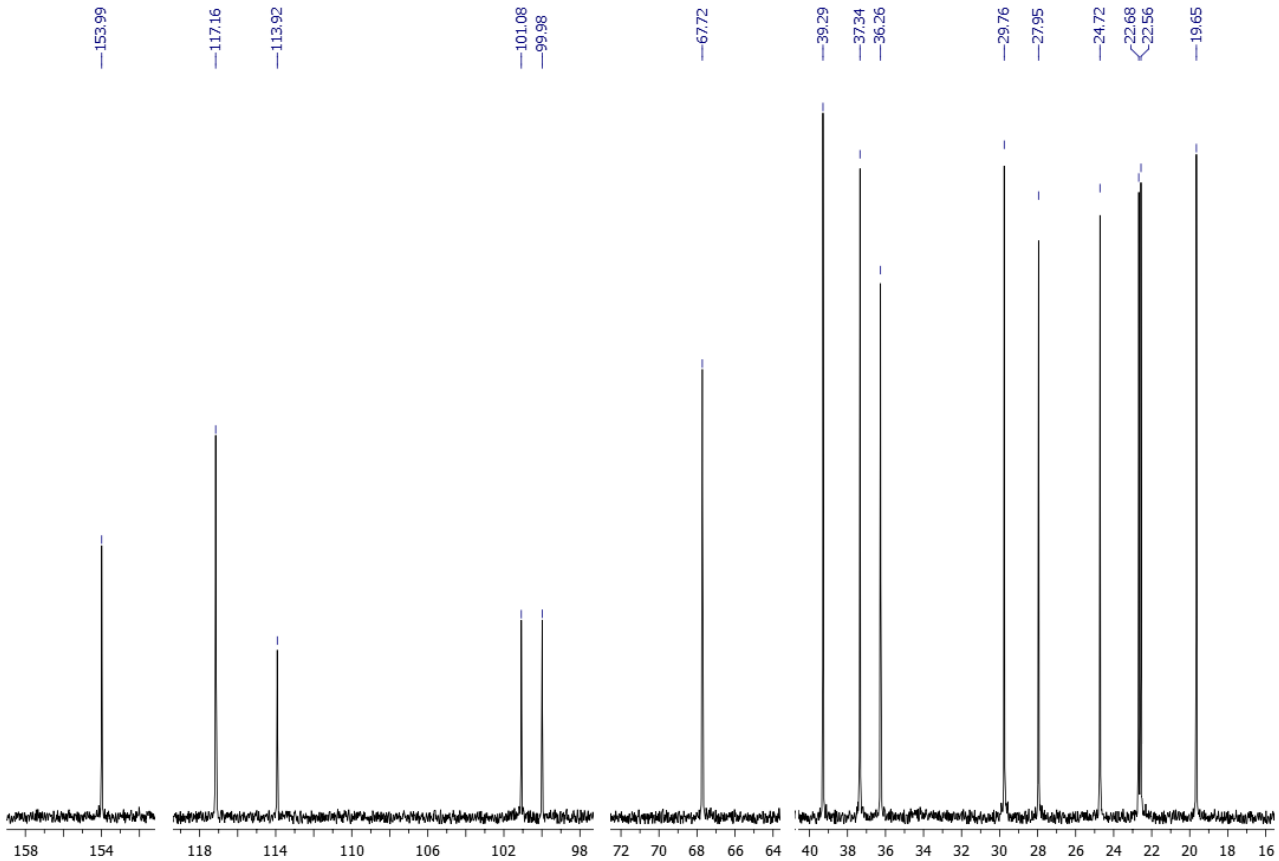


**Figure S23.** $^{13}$C-NMR spectrum (100 MHz, $CDCl_3$) of ((2,5-bis(((*S*)-3,7-dimethyloctyl)oxy)-1,4-phenylene)bis (ethyne-2,1-diyl))bis(trimethylsilane) (*S*,*S*)-**7**: full scale spectrum (top) and spectrum expansions (bottom).

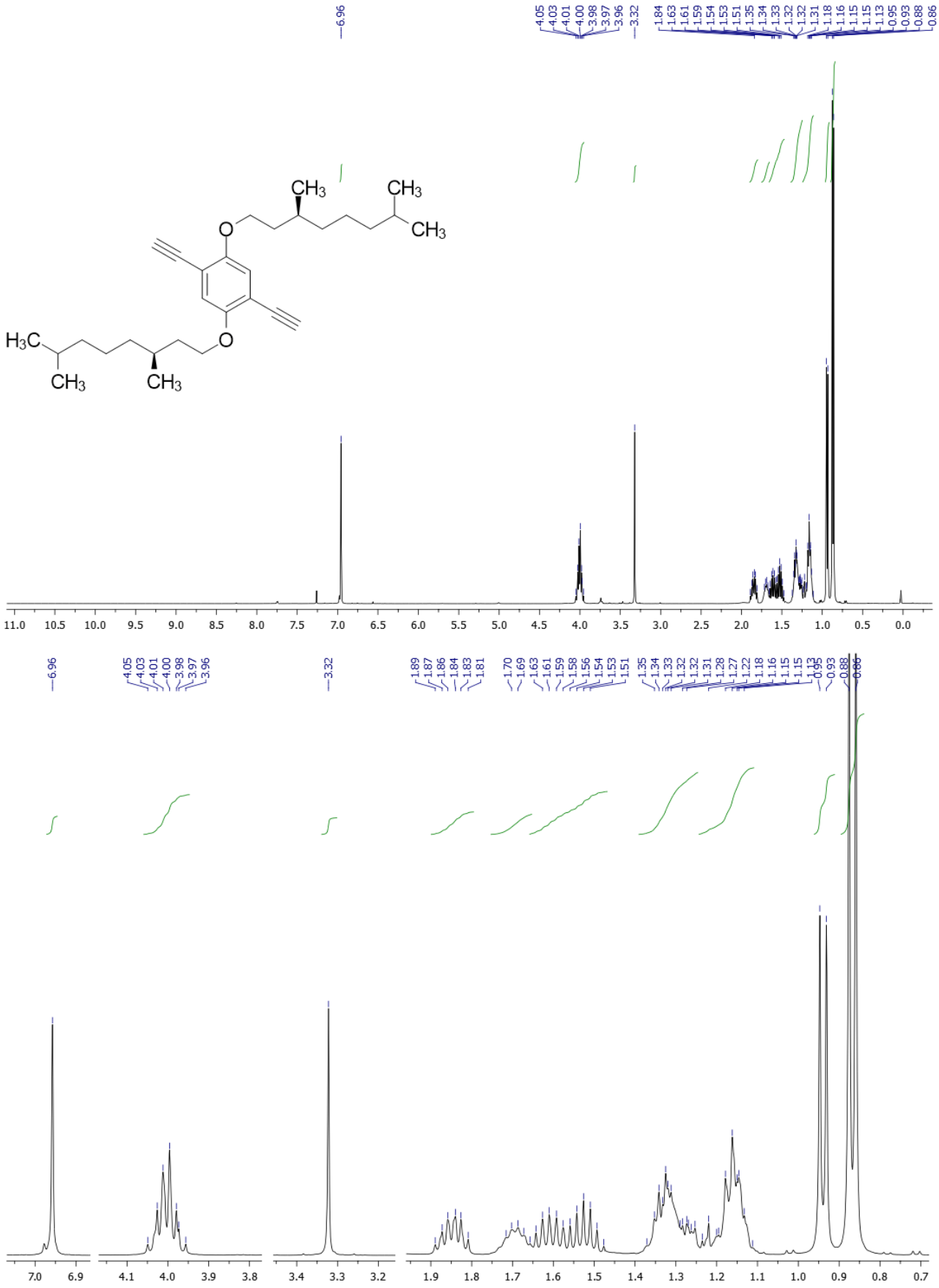


**Figure S24.** $^{1}$H-NMR spectrum (400 MHz, $CDCl_3$) of 1,4-bis(((*S*)-3,7-dimethyloctyl)oxy)-2,5-diethynylbenzene (*S*,*S*)-**8**: full scale spectrum (top) and spectrum expansions (bottom).

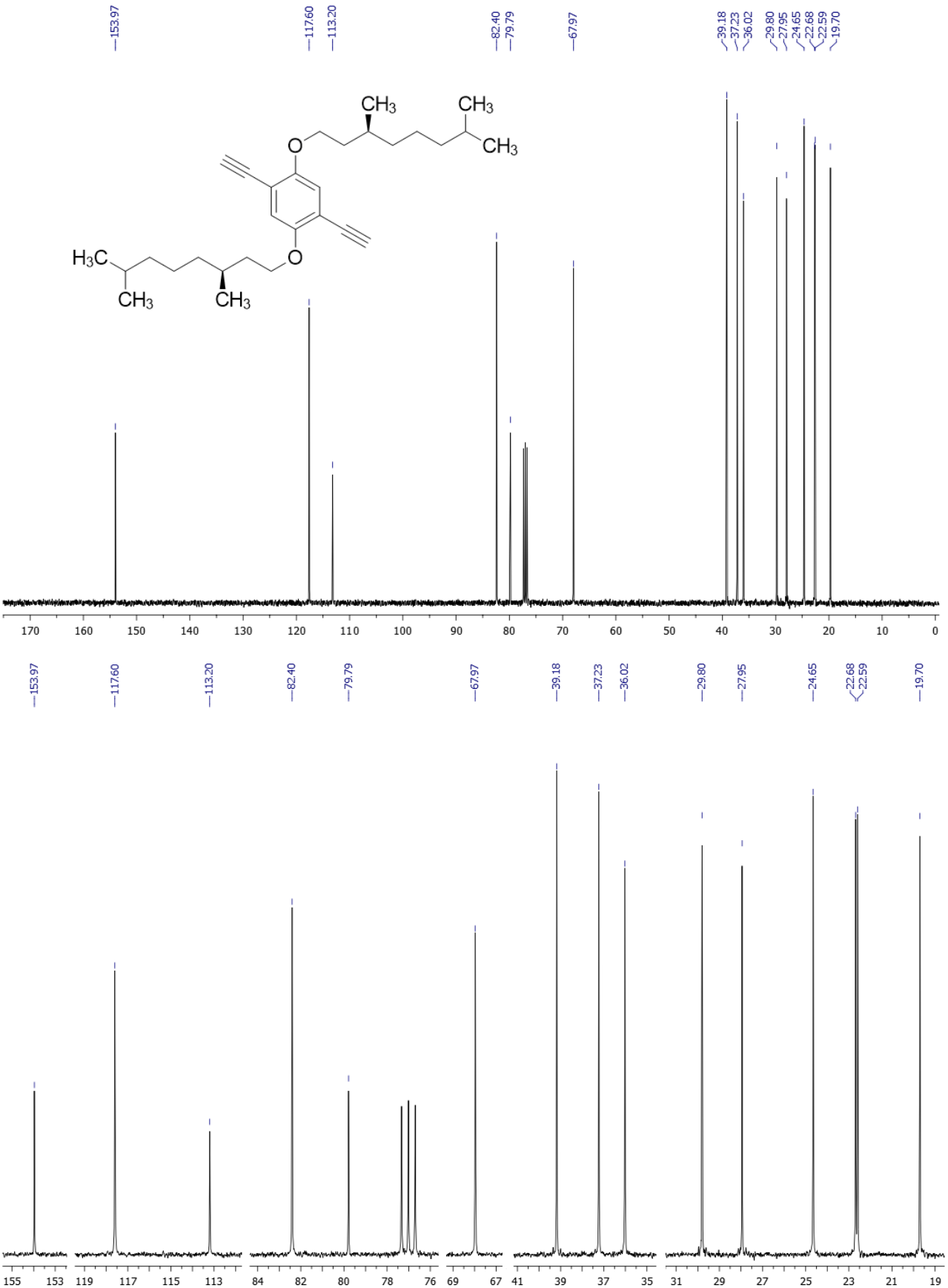


**Figure S25.** $^{13}$C-NMR spectrum (100 MHz, $CDCl_3$) of 1,4-bis(((*S*)-3,7-dimethyloctyl)oxy)-2,5-diethynylbenzene (*S*,*S*)-**8**: full scale spectrum (top) and spectrum expansions (bottom).

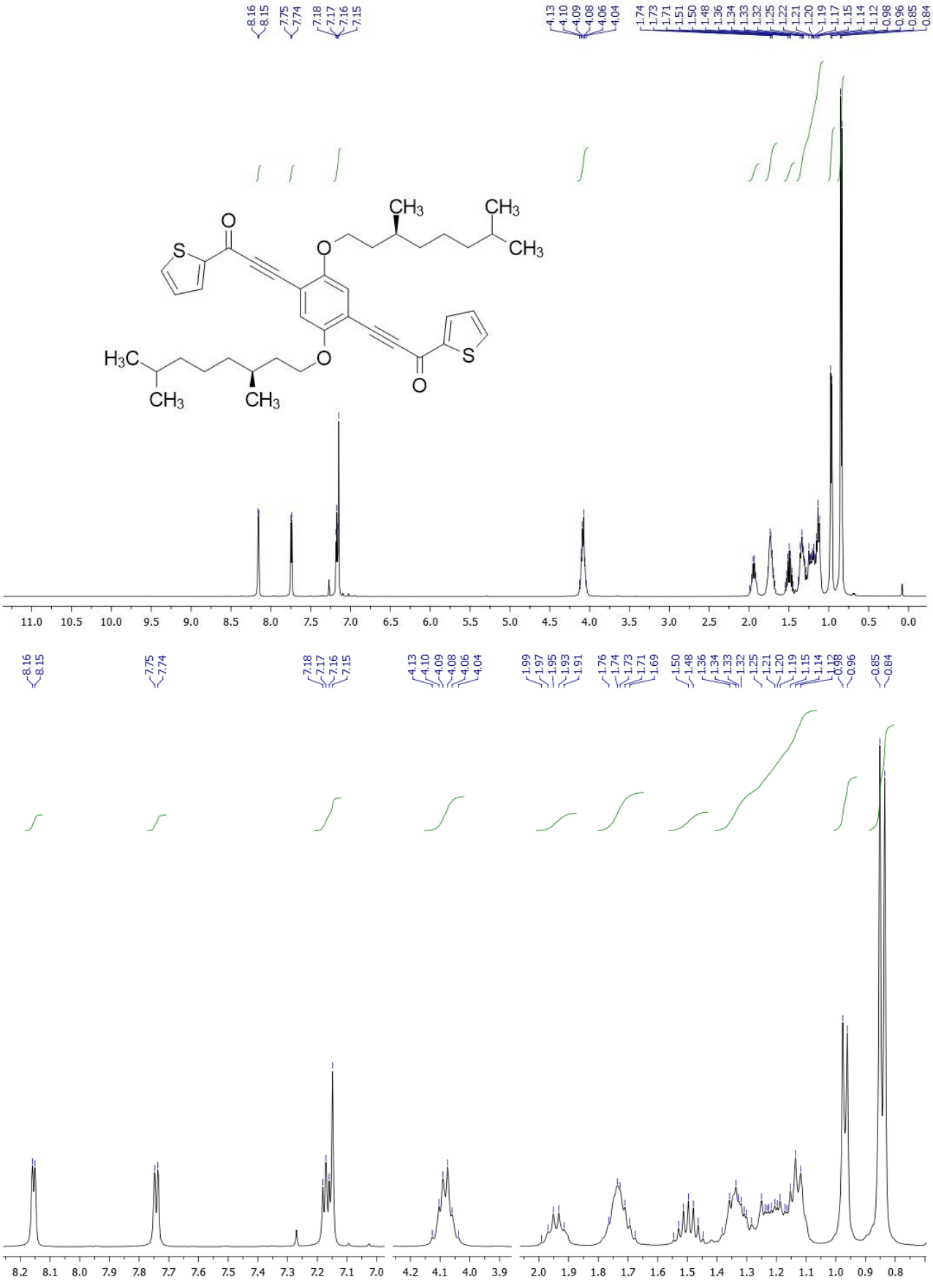
8.16
8.15
7.75
7.74
7.18
7.17
7.16
7.15
4.13
4.10
4.09
4.08
4.06
4.04
1.74
1.73
1.71
1.51
1.50
1.48
1.36
1.34
1.33
1.32
1.25
1.22
1.21
1.20
1.19
1.17
1.15
1.14
1.12
0.98
0.96
0.85
0.84
O
S
O
CH3
CH3
CH3
O
S
O
H3C
CH3
CH3
11.0 10.5 10.0 9.5 9.0 8.5 8.0 7.5 7.0 6.5 6.0 5.5 5.0 4.5 4.0 3.5 3.0 2.5 2.0 1.5 1.0 0.5 0.0
8.2 8.1 8.0 7.9 7.8 7.7 7.6 7.5 7.4 7.3 7.2 7.1 7.0
4.2 4.1 4.0 3.9
2.0 1.9 1.8 1.7 1.6 1.5 1.4 1.3 1.2 1.1 1.0 0.9 0.8

**Figure S26.** $^{1}$H-NMR spectrum (400 MHz, $CDCl_3$) of 3,3'-(2,5-bis((*S*)-3,7-dimethyloctyloxy)-1,4-phenylene)bis(1-(thiophen-2-yl)prop-2-yn-1-one) (*S*,*S*)-PTPO: full scale spectrum (top) and spectrum expansions (bottom).

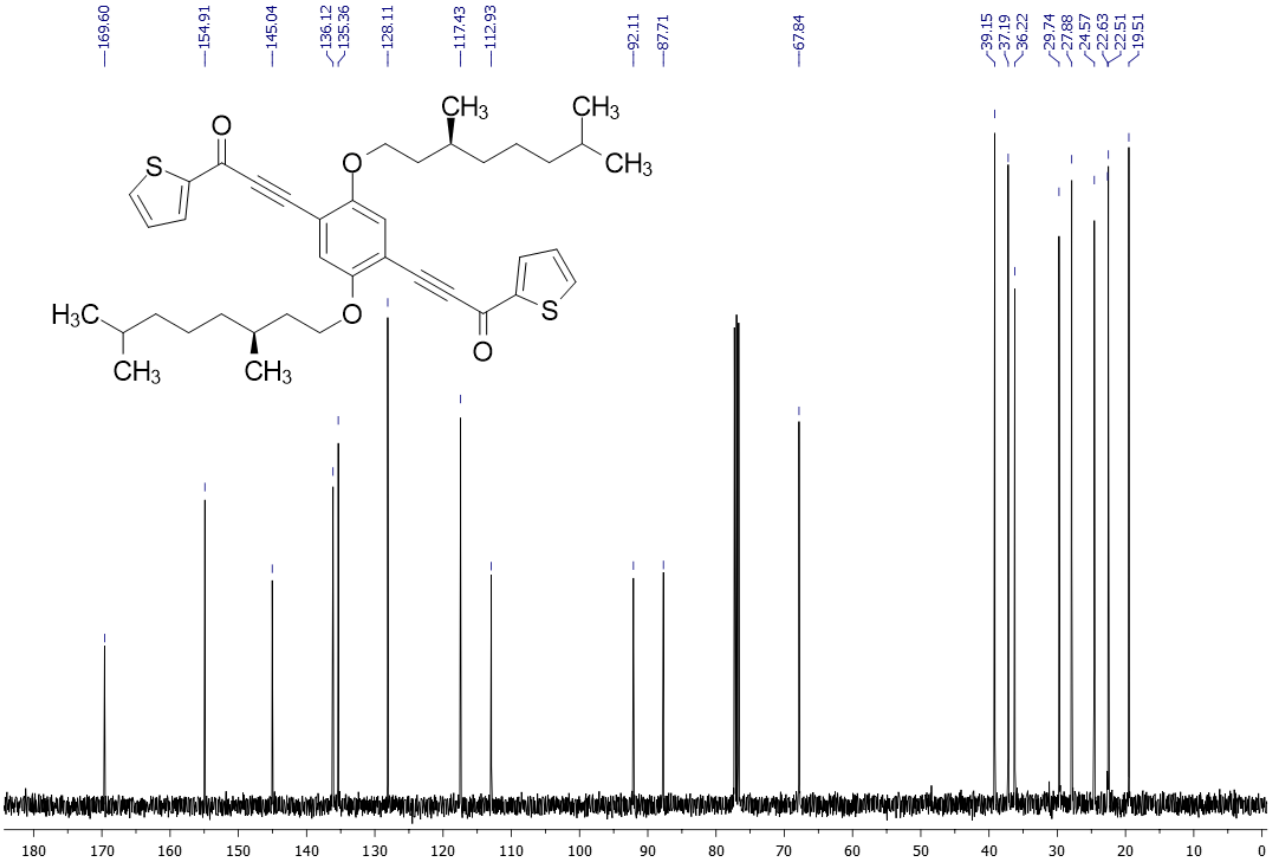

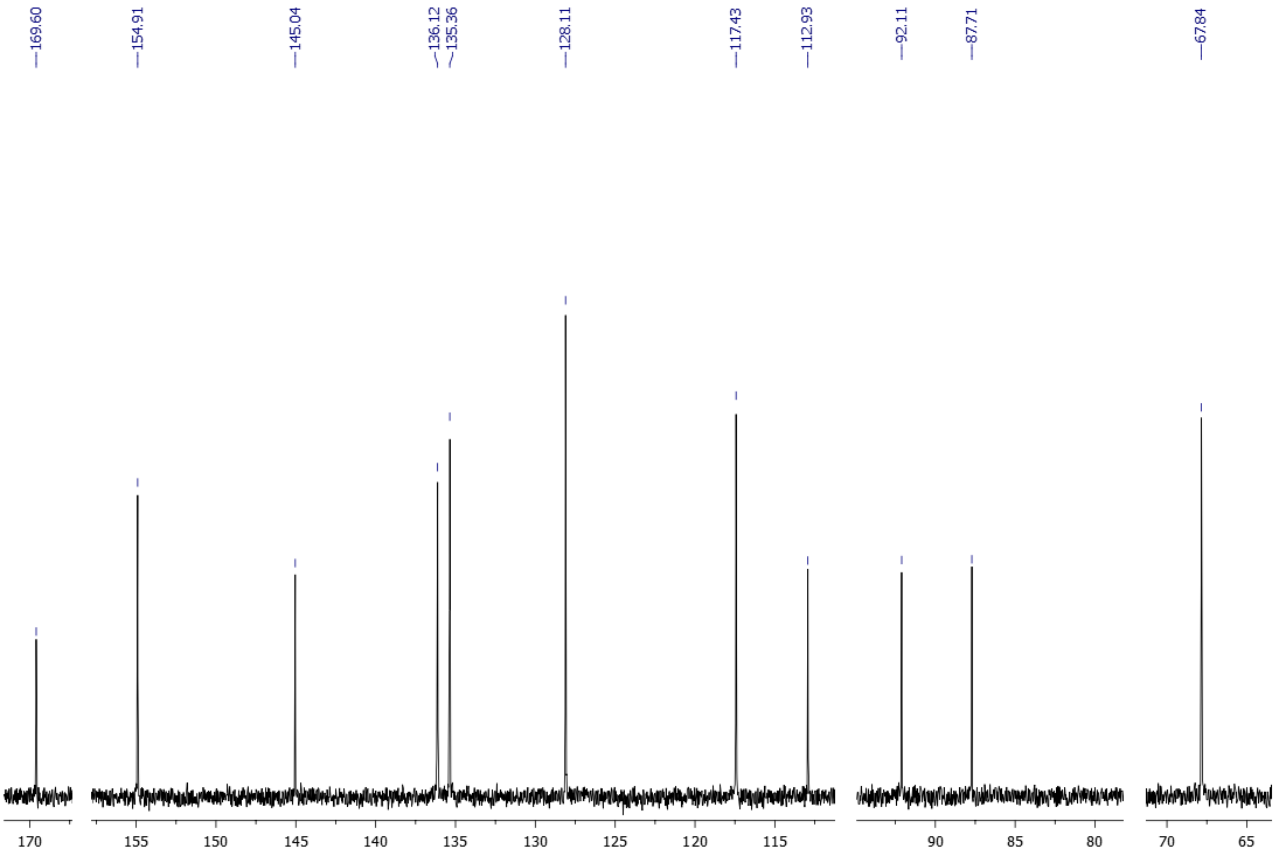


**Figure S27.** $^{13}$C-NMR spectrum (100 MHz, $CDCl_3$) of 3,3'-(2,5-bis((*S*)-3,7-dimethyloctyloxy)-1,4-phenylene)bis(1-(thiophen-2-yl)prop-2-yn-1-one) (*S*,*S*)-PTPO: full scale spectrum (top) and spectrum expansions (bottom).

## Supplementary references

[S1] G. Albano, M. Lissia, G. Pescitelli, L. A. Aronica, L. Di Bari, *Mater. Chem. Front.* **2017**, *1*, 2047.

[S2] G. Albano, F. Salerno, L. Portus, W. Porzio, L. A. Aronica, L. Di Bari, *ChemNanoMat* **2018**, *4*, 1059.

[S3] G. Albano, T. Colli, T. Biver, L. A. Aronica, A. Pucci, *Dyes Pigm.* **2020**, *178*, 108368.

[S4] F. Zinna, T. Bruhn, C. A. Guido, J. Ahrens, M. Bröring, L. Di Bari, G. Pescitelli, *Chem. Eur. J.* **2016**, *22*, 16089.